IN-FLIGHT MEASUREMENTS OF FREESTREAM ATMOSPHERIC TURBULENCE INTENSITIES

A Thesis

by

JOSHUA ALAN FANNING

Submitted to the Office of Graduate Studies of
Texas A&M University
in partial fulfillment of the requirements for the degree of

MASTER OF SCIENCE

Approved by:

Chair of Committee,	William Saric
Committee Members,	Edward White
	David Staack
Head of Department,	Rodney Bowersox

December 2012

Major Subject: Aerospace Engineering

ABSTRACT

The last key to implementing laminar flow control on swept-wings is controlling the crossflow instability. One promising technology is spanwise-periodic discrete roughness elements (DREs). Previous work has shown success with applique DREs and extending the region of laminar flow. This work seeks to extend the DRE technology to include dielectric barrier discharge plasma actuators as well as recreate past experiments with applique DREs.

One major need in implementing DREs and controlling crossflow is attaining an accurate measurement of the freestream atmospheric turbulence intensities. Knowing the atmospheric turbulence intensity will allow for comparing wind tunnel experiments to the flight environment and help produce better wind tunnel experiments by allowing them to better match the flight environment. Also, knowledge of the turbulence intensity at the specific instance of an experimental data point will allow for determining if differences in experimental results are the result of a difference in turbulence intensity. It has been determined through this work that the levels of freestream turbulence range from 0.023% - 0.047% with an average of 0.035%. These levels were reached through the use of temporal correlations to remove electronic noise as well as acoustic sound from the hotwire measurements and hence are lower than previously calculated.

DEDICATION

To my parents, I would not have been able to accomplish this without all of your support and encouragement through the years.

ACKNOWLEDGEMENTS

I would like to start by thanking my committee chair and advisor, Dr. William Saric, for allowing me this opportunity to work at the Texas A&M Flight Research Lab and learn the techniques of flight testing. I would also like to thank my other committee members, Dr. Edward White and Dr. David Staack, for their help and support in completing this work.

I would also like to think Lee Denham and Aaron Tucker, the pilots who got the airplane off of the ground and back safely every time. They both were always accommodating of scheduling the flights and put up with some demanding requests at times. I can't thank them enough for their work and the aviation knowledge they passed on to me.

Thanks also to the departmental staff that worked to keep everything going. To our mechanic, Cecil Rhodes, who made sure the airplane was always ready for flight. I am grateful for the knowledge of airplane maintenance he conveyed to me and for him allowing me to work on the airplane and get hands on experience. Also to Colleen Leatherman for all of her work without which the lab would not be able to function.

All of this work required a team effort, and I could not have accomplished this work without the help from other fellow graduate students. At the Flight Research Lab, thanks to Brian Crawford, Tom Duncan, Simon Hedderman, David West, and Tom Williams who all came in early in the morning to work flights. Also, thanks to Rob Downs for all of his help in getting the hotwires and the codes behind the measurements working.

Lastly, thanks to Alex Craig and Ray Humble who worked alongside on the plasma effort helping make the inserts and figuring out some of the fundamentals behind how the plasma actuators worked in order to attempt to make them work in flight.

Finally, I would like to acknowledge the grants that made this work possible: ATK Space Systems, Inc (prime sponsor NASA Langley Research Center) subcontract number PO-SP00029509 and Lockheed Aeronautical Systems Company (prime sponsor US Air Force Research Lab) PO#7189275.

TABLE OF CONTENTS

Page

LIST OF FIGURES

Page

CHAPTER I

INTRODUCTION

Studies into receptivity are critical to extending the effectiveness and knowledge of Laminar Flow Control (LFC). Receptivity is the process by which freestream disturbances enter into the boundary layer as fluctuations to the basic state and cause the transition from laminar to turbulent [1]. By stabilizing the boundary layer, delaying transition, and increasing the extent of laminar flow over a wing the drag can be significantly reduced, up to 15% [2], thus reducing the fuel consumption of the aircraft. One area of particular interest to LFC is in regards to swept-wings. The majority of large aircraft, which would benefit most from decreases in fuel consumption, have swept wings, so LFC on swept-wings is of most interest and will be discussed. A very detailed review and summary of swept-wing stability, transition, and receptivity, especially in regards to LFC, is provided by Hunt [3].

The LFC of particular interest for this work encompasses techniques to control the instabilities that occur on swept-wings. Multiple instabilities can be experienced upon a swept-wing model. Reed and Saric provide details of the basic instability mechanisms which can lead to transition on a swept-wing which include: Tollmien-Schlicting (T-S) waves, crossflow, attachment line contamination, and Görtler vortices [4]. While all of these instabilities are possible on swept-wings, most can be avoided depending on the design and installation of the swept-wing. Carpenter and Hunt provide ways to avoid these instabilities. Attachment-line contamination can be avoided by keeping the leading

edge radius below a critical value and by having an airfoil with free ends such that it is not in contact with any turbulent boundary layers. Görtler vortices can be avoided by avoiding concave curvature. T-S waves can be avoided by incorporating a favorable pressure gradient [5][3]. Crossflow instability is the only remaining instability, which cannot be easily controlled or eliminated simply via airfoil design without destabilizing other instabilities. Saric describes that crossflow is seen only on swept-wings because a velocity profile perpendicular to the inviscid streamlines is created due to a combination of chordwise pressure gradient and sweep. This inflectional profile is composed of co-rotating vortices that are aligned with the inviscid streamlines [6]. The crossflow instability can be dominated by either travelling or stationary waves depending on the level of freestream turbulence [7]. The level of freestream turbulence also influences the sensitivity to surface roughness [3]. Therefore, one of the keys to performing receptivity and LFC studies is having a measurement of the freestream turbulence. It is already well known that the flight environment is a very low turbulence environment, although past studies have left work to be done in determining just how low, leading to the crossflow instability being dominated by a stationary wave. It is the goal of this work to further LFC in controlling stationary crossflow and determining just how low turbulence the flight environment actually is.

Discrete Roughness Elements

The Swept-Wing In-Flight Testing, SWIFT, model used for the current experiment was designed such that T-S waves are stabilized, Görtler vortices are eliminated, and attachment-line contamination is eliminated resulting in the only remaining instability

being crossflow [5]. One proven method for LFC on an airfoil dominated by stationary crossflow is the use of spanwise-periodic discrete roughness elements (DREs) [6][5]. Thus, SWIFT provides a desirable test bed for determining the effectiveness of DREs. The goal of this work was to extend the capabilities of DREs by introducing new technologies while comparing their effectiveness to existing technologies.

Applique DREs

Applique DREs have previously been found effective at delaying transition and have been used in a number of experiments. Saric reports of delaying crossflow dominated transition by using a DRE spacing less than the most critical wavelength in a wind tunnel environment [6]. Most significant to this research is Carpenter who showed applique DREs to work in-flight on the same platform used in this work [5]. Applique DREs are dry transfer dots that are typically 6-18μm in height that are placed at a wavelength subcritical to the most unstable crossflow wavelength. The DREs are placed at wavelengths subcritical to the most unstable wavelength because, as Riebert et al. showed, the use of DREs allows only crossflow waves that are integer multiples of the forced wavelength to grow and that no subharmonic wavelengths are destabilized [8]. For SWIFT, the most unstable wavelength is 4.5mm [5]; therefore the DRE spacing of most interest is 2-3mm. Due to the small spacing between the DREs, the typical diameter of applique DREs used on SWIFT is 1mm. In order to get the height necessary, multiple layers of DREs can be applied. Applique DREs are a tested and proved method that can be used to verify the experimental setup.

Plasma DREs

With all of the work done with applique DREs, a new technology is needed to further the use of DREs and increase their technical readiness level. One promising technology is the use of dielectric barrier discharge (DBD) plasma actuators. DBDs have been used in the past for different types of flow control including: turbulent boundary layer separation control, leading-edge separation control, dynamic stall control, circular cylinder wake control among many others [9]. Saric and Reed mention the effectiveness of plasma actuators in a low-speed wind tunnel [10]. Schuele shows plasma actuators are effective at Mach 3.5 flows [11]. Corke explains that DBDs work by generating a body force vector that couples with the momentum of the external flow [9]. The theory behind the current work is that the disturbance caused by the DBDs can be spaced at a wavelength subcritical to the most unstable crossflow wavelength and therefore be used as DREs and a replacement for applique DREs.

Hotwires

Overview and Motivation

The end goal of the majority of this compilation of work performed here and by others is to form some set of criterion for applying LFC techniques to a general aircraft wing. In order to reach that goal, some level of flight testing will be required of techniques that are effective in the wind tunnel environment, but one of the main differences between the wind tunnel environment and the flight environment is the freestream turbulence intensity. While widely accepted that the flight environment has lower turbulence than the majority of wind tunnels, just how much lower is not fully known. A detailed analysis of the freestream atmospheric turbulence in-flight is needed

to aid in knowing more about the environment in which aircraft operate, but also to make further progress with wind tunnel experiments [12].

Freestream disturbances are composed of both rotational (turbulence) and irrotational (sound) disturbances that affect either the crossflow or T-S instability, respectively [1]. One of the keys to analyzing freestream turbulence is to separate the sound from the actual freestream turbulence [13], along with the removal of any electronic noise in the signal. Also of value would be an analysis of if and how the freestream atmospheric turbulence varies with respect to the time of year or geographic location.

In order to measure the freestream disturbance, a technique is needed that is capable of measuring small velocity fluctuations. A hotwire is best suited for this. Hotwire anemometry is suitable for measuring velocity fluctuations $O(10^{-3}U_\infty)$ [1], This level is sufficient for measuring fluctuations due to freestream disturbances. Saric lists keys to reporting turbulence measurements in order to better define the environment under which the measurements were taken. Saric included defining the bandpass spectrum used on the signal, unit Reynold's number at which the data was taken, correlations to remove turbulence from sound, and *u'*, *v'*, and *w'* measurement [14][15].

Current Status

Previous work has been done to determine freestream atmospheric turbulence intensity (*Tu*). Carpenter measured *Tu(u')* = 0.05-0.07% (bandpass: 1Hz-10kHz) at altitudes from 3,000-10,500ft and airspeeds from 158-168KTAS in a previous study on the same platform as was done in this study [5]. Riedel and Sitzmann measured *Tu(u')* = 0.034 – 0.048% (no bandpass, select spectral editing) at altitudes from 17,700-21450ft

and speeds from M = 0.45-0.57. They also found that turbulence intensity is independent of airspeed under still air conditions, which are defined as flights where no influence of turbulence is felt in flight [16]. One of the downsides to both of these experiments is that no effort was made to remove either electronic noise or acoustic sound from the measurements. However, Riedel and Sitzmann did perform discrete power spectra editing to remove spikes that were produced from their power supply system but did notice other electronic noise from other unknown sources. Riedel and Sitzmann noted that at very high power settings turbulence intensities increased which was believed to be caused by airframe vibrations induced by the engines, but these results were not reported in the final range of turbulence levels. This result caused significant issues that are incurred by almost all aircraft used to measure freestream turbulence because the measurements must be independent of the platform used. This independence is necessary since turbulence is a weather phenomenon and not in any way related to the aircraft being used [12]. Therefore, a platform is needed that can either achieve the desired speeds for turbulence measurements without excess airframe vibration or have a way to remove any noise in the signal caused by the aircraft. A useful result from both of these prior studies was that the measured in-flight turbulence intensities were around or below the bound of $Tu < 0.05\%$ recommended by Saric and Reshotko for receptivity experiments [17].

CHAPTER II

DATA ACQUISITION

The instrumentation and data acquisition programs for this series of flight tests varied throughout the campaign due to upgrades to the existing system. The author will therefore detail the entire system used and include all instrumentation used.

Instrumentation

Computer and Data Acquisition System

The initial setup to acquire all of the flight data was through a National Instruments (NI) PCI-6071E and NI-PCI-6723. The NI-PCI-6071E is a 12-bit data acquisition (DAQ) board with 32 differential analog inputs at a maximum sampling rate of 1.25MHz and 2 analog outputs. The NI-PCI-6723 is a 13-bit DAQ board with 32 analog outputs. Inputs were connected to the NI-PCI-6071E using a NI-BNC-2110 and NI-BNC-2115 which provide 8 and 24 BNC analog inputs, respectively. This system was replaced with a pair of 16-bit DAQ boards that are USB based. The NI-USB-6259 Mass Term offers 16 differential inputs at a maximum aggregate sampling rate of 1MHz and 4 analog outputs, and the NI-USB-6255 Mass Term offers 40 differential inputs at a maximum aggregate sampling rate of 750kHz and 2 analog outputs. This new setup offered multiple advantages including increased resolution offered by the 16-bit boards, compatible with existing BNC boards using mass terminal cables, capability of sampling channels at two different frequencies, and USB connectivity. USB connectivity is

exceptionally convenient because it removed conflicts across the laptop computer's PCICMA bus.

Multiple computers were used throughout this set of experiments, starting with a Dell M65. The Dell M65 ran Windows XP on a dual core Intel Core Duo 2.00GHz processer, 2GB of memory, and a 128GB SSD. This computer was run until the DAQ system upgrade because it was the only laptop available that did not have software conflicts with running the PCI based instrumentation suite. Upon upgrading the DAQ system, the laptop used for flights was upgraded to a Dell Precision M4400 running Windows 7 on a quad core Intel Core 2 Extreme 2.54GHz processor, 4GB of memory, and a 128GB SSD. This computer was run on flights until an upgrade was made to the IR camera. Then, a Panasonic Toughbook CF-52 running Windows 7 on a dual core Intel Core i5-2540, 2.60GHz processor, 16GB of memory, and a 256GB SSD was used for all flight operations.

Since laptops were used for these flight experiments, due to the inconvenience of using desktops in a small aircraft, a converter was required to connect to the PCI based systems which consisted of the two previously mentioned DAQ boards and a video capture card used in conjunction with the FLIR SC3000 IR camera. The solution to this was a Magma PCI-PCICMA bridge. While using the PCI based DAQ system, a Magma 4-slot PCI-PCICMA bridge was used, but once the DAQ system was upgraded to the USB system a Magma 2-slot PCI-PCICMA bridge was used. Swapping to the smaller bridge allowed for a decrease in instrumentation weight and an increase in usable space on the instrumentation rack. However, upon a later upgrade of the IR camera, the

Magma 2-slot PCI-PCICMA bridge was removed as there were no longer any PCI based equipment on the aircraft

IR Camera

The next major upgrade to the flight hardware was an upgrade to the IR camera used in flight. The initial camera used was a FLIR SC3000 which offered a 320x240 pixel resolution and a spectral resolution in the 8-9μm spectral range. This was replaced with a FLIR SC8000 that has a 1024x1024 pixel resolution and a spectral resolution in the 3-5μm spectral range. The SC8000 boasts many features over the SC3000 including gigabit Ethernet connectivity instead of PCI and serial, a maximum frame rate of 132Hz instead of 50Hz, and a pixel density increase of over 1200%. The increase in pixel resolution is the most valuable improvement and is extremely noticeable in the IR images and provides a much more detailed picture of the transition location, as can be seen by comparing Fig. 1 and Fig. 2.

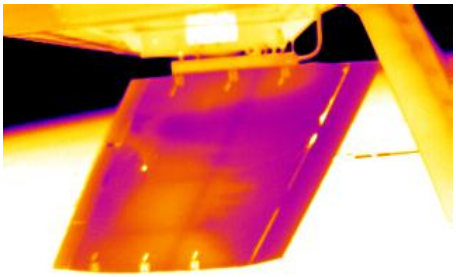

Fig. 1 Picture output from FLIR SC3000. Picture is scaled to 70% but otherwise unedited.

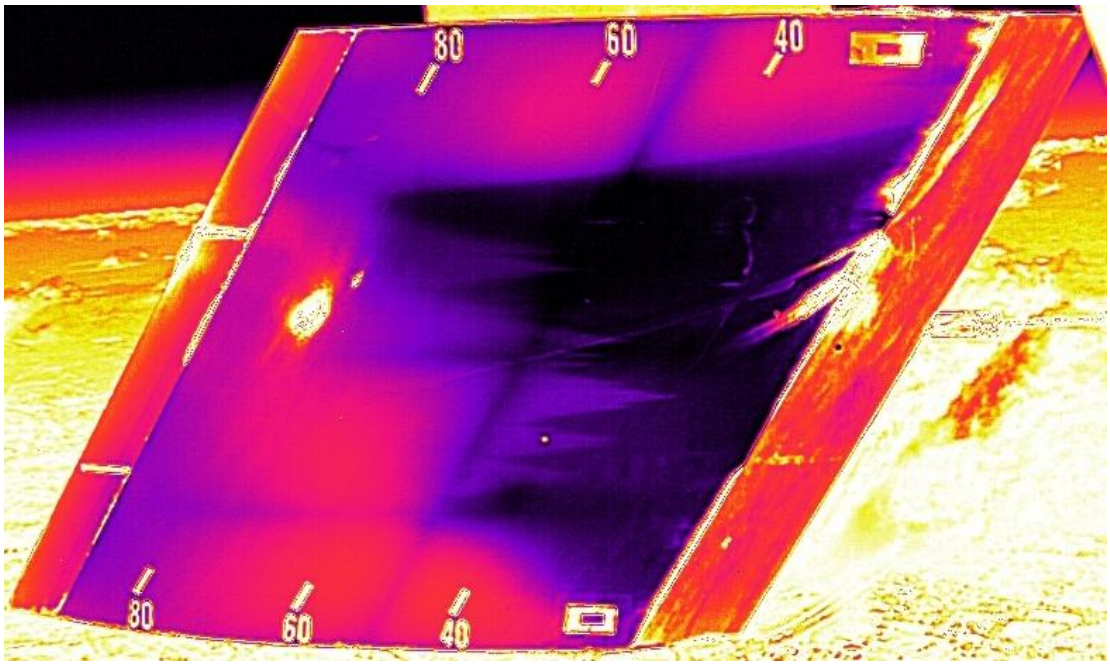

Fig. 2 Picture output from FLIR SC8000. Picture is scaled to 70% and cropped to show only the SWIFT model.

Air Data

Instrumentation for collecting all of the air data during flights was also installed in the aircraft. For air data collection an Aeroprobe, conical tip, five-hole probe was used to measure static pressure, dynamic pressure, angle of sideslip (β), and angle of attack (α). The pressures from the five-hole probe were measured using four Honeywell Sensotech FP2000 pressure transducers, that offered 0.010% accuracy, installed inside of the SWIFT model. Static pressure was measured on a transducer with a range of 0-15psia, and the other pressures were measure on transducers with a range of ±2psid. Total temperature was also measured using an Omega CNi32 temperature controller. Initially hooked to the controller was an Omega 100 ohm, 3-wire RTD which was later replaced with a SpaceAge Control 4222-08 500 Ohm, 3-wire RTD as seen in Fig. 3.

Fig. 3 Total temperature probe.

Pilot Display

Initially the pilots had both a digital display and LCD display to provide β and chord Reynolds number (Re_c) during flight. However, the digital display was removed during this set of experiments. The display was no longer needed because of the presence of the LCD display to provide the pilot's data. There was also a lag in data transmission to the digital display since its signal was sent back out of LabVIEW via an analog out on one of the DAQ boards to go to the display. The LCD display was just an extended monitor on the laptop so it was a direct view of the LabVIEW front panel and did not require a signal to be sent back out through the DAQ board. Also, removal of the digital display cleared up real estate above the dash on the aircraft to provide a less impeded view out of the windshield.

Hotwire Instrumentation

For the collection of hotwire data, an AA Labs AN-1003 constant temperature anemometer was used. Output signals from the anemometer were filtered through a Krohnhite Model 3016 bandpass filter. A Tripp-Lite LC1200 line conditioner was used between the 120V inverter and both the anemometer and filter. While the Exeltech XP-1100 power inverter used was a clean sine-wave inverter and met the recommendations for use with hotwire anemometry in an aircraft [12], the line conditioner was used to further prevent any electronic noise or error added to the hotwire measurements due to the power supply to the hotwire instrumentation Also, a Tektronix TDS2014C oscilloscope was installed in order to tune the damping of the hotwires in-flight.

Data Acquisition Program

All data acquisition was performed using LabVIEW 2009. The code was originally written by Carpenter [5] and later modified by Woodruff [18] prior to the current author taking possession of the code. The displays will be detailed starting at the time when the current author took possession. The data acquisition program was under constant evolution, often being changed and improved on a weekly, sometimes daily, basis. This section will provide an overview of some of the modifications made and lessons learned. Also included is information relating to acquisition and post-processing of hotwire data, whose theory and calculations are provided in a later chapter.

The front panel to the LabVIEW virtual interface consisted of two separate sections, a pilot display and an FTE display. Both were a part of the same screen, but an extended monitor setup was used on the laptop in order to provide the pilot their display on their

yoke mounted LCD display. Figure 4 shows the full front panel display with both the pilot and FTE displays in its final form. The two displays are separated by a vertical purple line which allows the FTE to properly align the front panel on the laptop display. Both the pilot and FTE displays will be detailed separately, including iterations and modification made during the flight testing program.

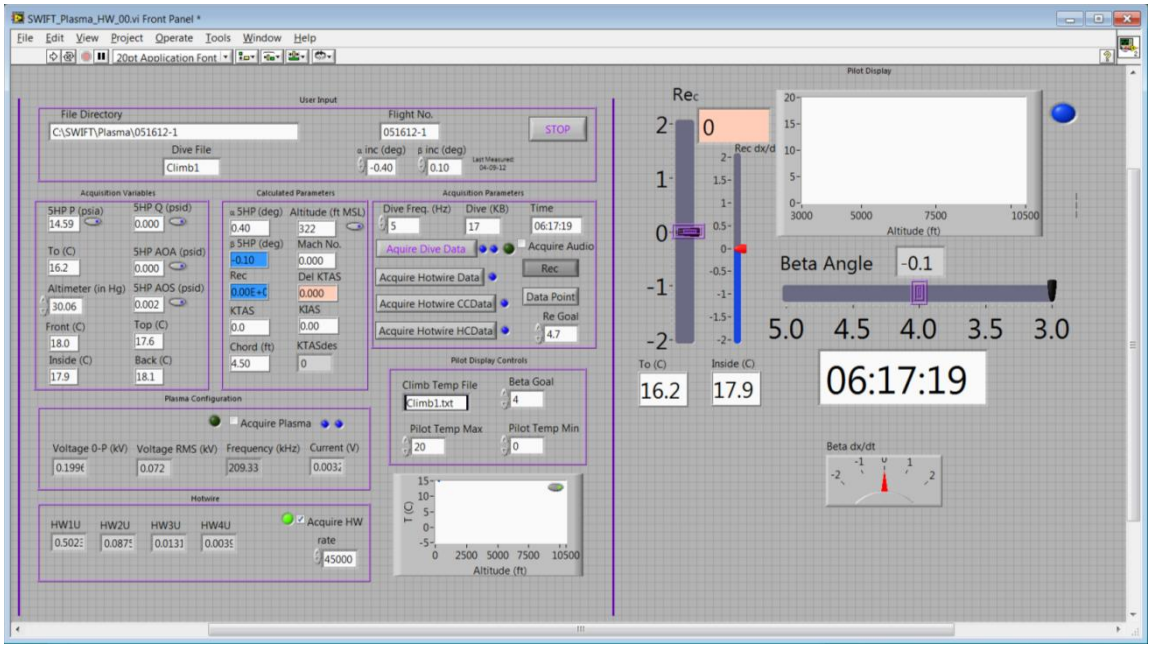

Fig. 4 LabView Front Panel, including FTE (left) and pilot (right) displays.

Pilot Display

As mentioned above, the pilot used both a digital display and LCD display; however, this section will only deal with the LCD display. The original design of the pilot LCD display contained simply a slider for Re_c and β, a light indicating data was being acquired, and sliders displaying rate of change in Re_c and β as can be seen in Fig. 5.

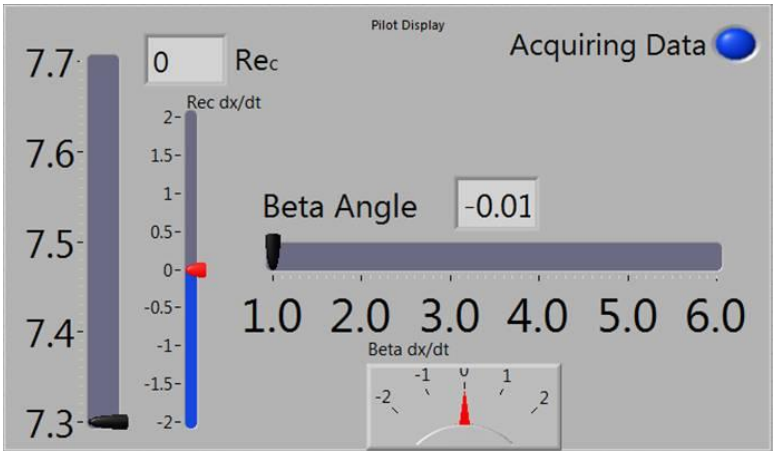

Fig. 5 Initial pilot display.

The first major change to the display was changing the scaling of the Beta Angle slider. As Fig. 5 shows, the initial display was static and provided a 5° range in β. It was desired, however, that the pilots hold β to within ±0.1° of the designated β and this display does not provide that resolution. Therefore, the Beta Angle slider was manually adjusted with a range of ±0.2° centered on the desired β, as shown in Fig. 6. This setup provided the pilots with enough resolution to fly within ±0.1° of the desired β.

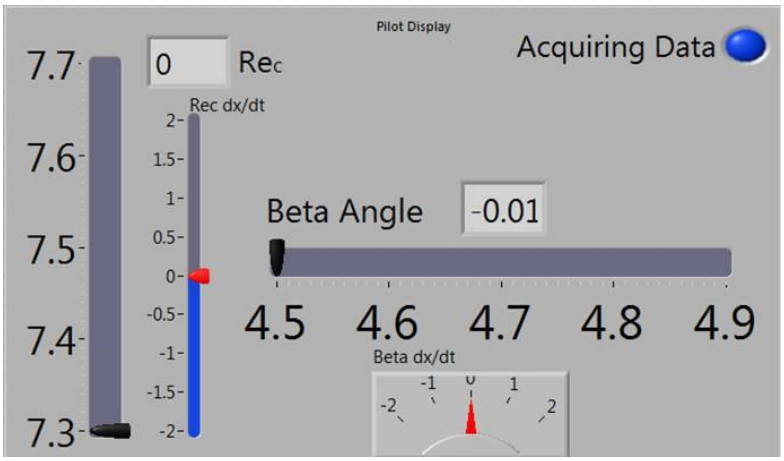

Fig. 6 Pilot display with centered Beta Angle.

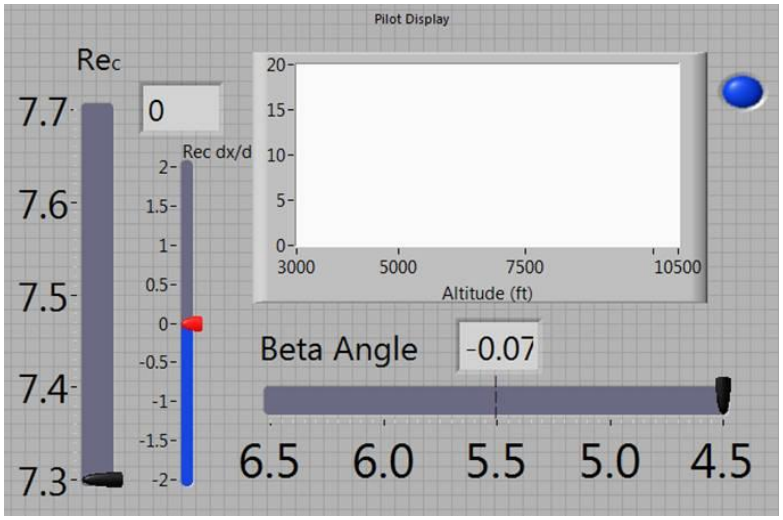

Fig. 7 Pilot display with temperature display.

The next change to the display was two-fold, shown in Fig. 7. First the scaling for the Beta Angle was changed to a range of ±1° which allowed the pilots to track β into the desired point from farther off condition, which was most useful when changing β during the research dive. Also, a temperature plot was provided to the pilot. Initially the temperature plot was provided to the pilot to allow them to see where the temperature

profile inverted during the climb out. This allowed them to anticipate the resulting change in Re_c and know not to try to correct for the rapid changes because Re_c would recover on its own. An added benefit to this display was that it was scaled to end at 3000ft which corresponds to the minimum altitude allowed for research portions of the flights. This allowed the pilots a reference on their display to know when the end of the dive was approaching, rather than having to constantly look up to check the altimeter. Even with the ability to report altitude on the pilot display, the aircraft altimeter was regarded as the truth source for all altitudes and was used to determine when the research dive was to be terminated. It should also be noted that the rate of change indicator for Beta Angle was removed in this iteration on the pilot display. Neither the Rec nor Beta Angle rate of change indicators worked as originally hoped so the indicator for Beta Angle was removed in order to make room for the temperature plot.

Following the addition of a temperature plot was the addition of displays for both the air temperature and the interior surface temperature of SWIFT, as shown in Fig. 8. This addition did not prove as useful as some of the other additions. It was added mainly because the capability was available, but the displays were never used much by the pilots. Companion displays were used by the FTE on their screen as a tool to determine if the model had been cold soaked long enough as it provided a comparison of the outside air temperature and the interior of the test side of the model. This information was left on the pilot display in case they desired the information.

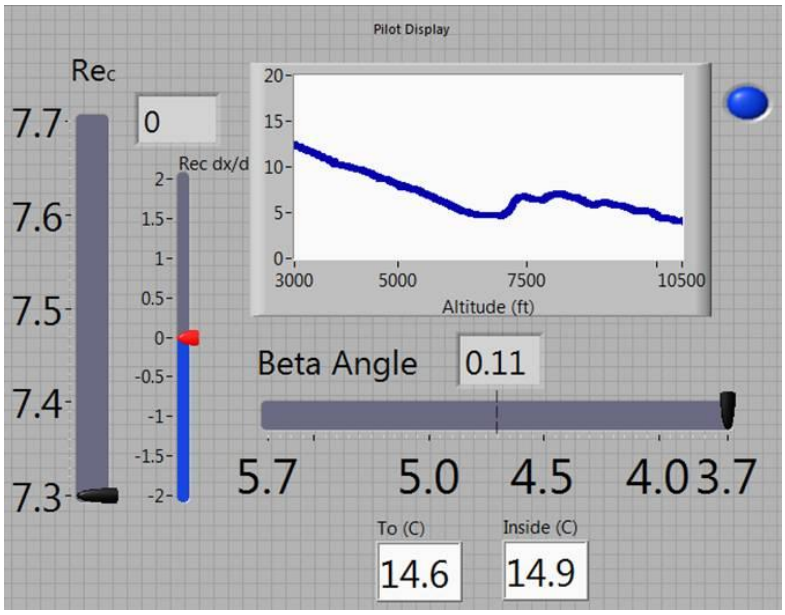

Fig. 8 Pilot display with air and model temperatures.

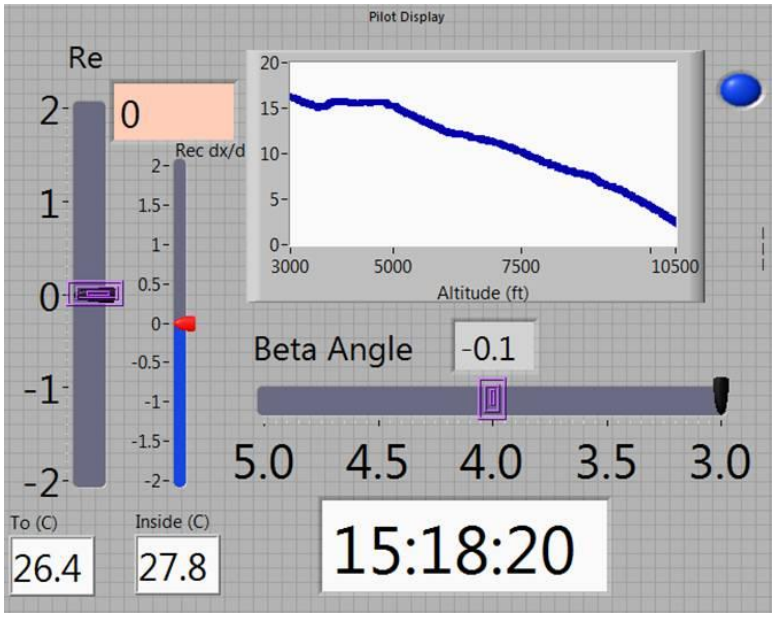

Fig. 9 Final pilot display iteration.

The final major iteration on the pilot display provided many additions that increased both aircraft safety and pilot proficiency. Items added to the display can be seen in Fig. 9 and include: indicators for the center of the Rec and Beta Angle slider, a time display, changeable scaling on the Rec slider, and background color change to the Rec number display. Indicators were added to the center of the sliders to allow the pilot to know more precisely where the center is located. The indicators were slightly larger than the slider's marker and allowed for the marker to be located under the indicators when on condition. At first this may seem like a trivial addition but, as can be seen in Fig. 8, LabVIEW does not always provide numerical indicators on the slider evenly and the pilots could be left guessing as to the exact location of the center of slider. A clock was added to the display because during a few flights pictures were taken with a digital camera with the co-pilot writing down timestamps of when the pictures were taken in order to go back and match the picture with the corresponding air data conditions. It can be seen when comparing Fig. 9 to any of the other pilot display pictures that the scaling and label on the Rec slider were different. The scaling was different because in Fig. 9 the Re slider was not set for to display Re_c but rather the difference in KTAS. The label was also changed to indicate that the slider does not display solely Re_c, but it was felt that it was appropriate to leave the label as Re since the difference in KTAS displayed was based off of flying a desired *Re'*. A display of the difference in KTAS was needed to perform the hotwire calibrations. Finally, it was incorporated within the LabVIEW code to change the background color of the Re number display to a shade of red when KTAS crossed either a lower or upper bound. This addition was needed to prevent the pilot from overspeeding

or stalling the aircraft during the hotwire calibrations. During the calibrations the pilots were focusing on flying KTAS, while all of the aircraft limits are KIAS so the pilots could easily fly the aircraft past its limits without realizing it. Having an indication of when the aircraft was reaching its operational limits on the LabVIEW displays allowed both the pilot and FTE to know that the aircraft's airspeed indicator needed monitoring.

FTE Display

The FTE display is much more involved than the pilot display as it provides the FTE with a readout of almost every acquisition variable along with many calculated properties. This was necessary to allow the FTE to monitor the system during flight and discover any anomalies that may occur, whereas the pilot only needed to know the values critical to flying the aircraft in order to reduce their workload and prevent distraction from extraneous indicators. Therefore due to its size and layout, the FTE display will be discussed in its individual parts and then a brief discussion on the evolution and lessons learned of the display.

In order to provide the best explanation of all of the components of the FTE display, the final evolution of the display, as shown in Fig. 10, will be discussed as it contains all of the parts used throughout this flight test program and does not include a lot of the indicators used in past research that are no longer useful. The best way to describe all of the different inputs and variable will be to break the display down into its different components which are outlined by purple rectangles with labels above them.

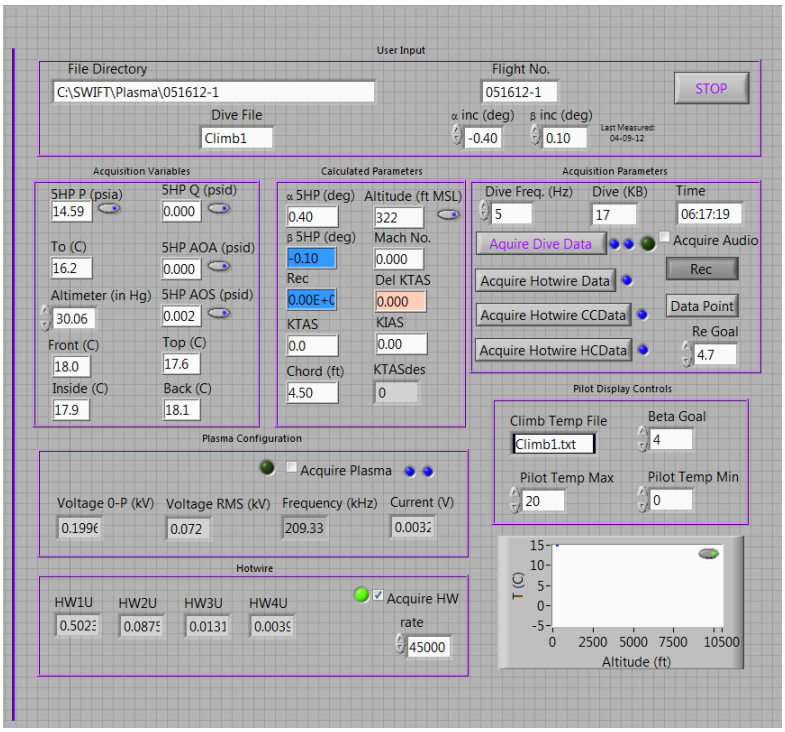

Fig. 10 Final FTE display.

The first sections is the User Input section which provides the FTE the ability to provide all of the file locations and naming identifications for all of the flights along with the different sections of the flight. It also contains the inputs for the measured offset between the five hole probe and the SWIFT model and the STOP button for the program.

Inside of the Acquisition Variables section are the indicators for the static, dynamic, angle of attack, and angle of sideslip pressures from the five hole probe. It also contains readouts from four thermocouples placed in different locations on the SWIFT model and from the total temperature probe installed on the underside of the port wing. Also included is an input for the local altimeter setting. This feature allows for zeroing the

offset or drift of the static pressure transducer based off the known atmospheric pressure. Buttons were provided beside the four pressure readouts to allow for zeroing out any drift that might occur in the pressure transducers; however, only the static pressure needed to be provided with an exterior reference value because it was an absolute pressure transducer while the other three were differential pressure transducers. Any drift in the transducers was removed during the preflight procedure while the airplane was inside the hangar with the hangar doors closed to ensure air flow did not affect the differential measurements.

The Calculated Properties section provides a readout for the properties that were calculated using the Acquisition Variables including the angles of attack and sideslip of the airplane relative to the SWIFT model, Re_c, true airspeed in knots, SWIFT chord length corrected for angle of attack, altitude, Mach number, and indicated airspeed in knots. A button was provided next to the altitude to correct the altitude for the current sea level pressure, similar to that used by the pressure transducers. Two other indicators were provided, Del KTAS and KTASdes, which were used for the hotwire calibrations and measurements. KTASdes provided the desired true airspeed in knots based on the necessary unit Reynold's number for a particular test condition. Del KTAS provided the difference between KTASdes and the actual true airspeed. It should also be noted that Del KTAS had the same trigger to change the indicator background color upon passing an upper or lower bound in true airspeed as the pilot's Re slider mentioned earlier. This functionality was provided to the FTE in addition to the pilot in order to provide a redundancy and have multiple people monitoring the airspeed.

Next is the section that provides controls for all of the Acquisition Parameters involving mostly the output files. Provided within this section was a control to control the frequency at which data was written to the main output file, an indicator for the size of the main output file, and an indicator of the time. Also provided was the Re Goal control which controlled what the necessary unit Reynold's number was for each test condition and is what controls the KTASdes and Del KTAS. Re Goal also controlled the value the pilot's Re slider was centered about. The Acquire Dive Data button controls when data was written to the main output file. Buttons were also included to dictate which of the different hotwire measurements was currently being acquired, which were, in order from top to bottom, the actual hotwire measurements, hotwire cold calibration measurements, and hotwire hot calibration measurements. Lights were provided beside all four of these buttons to give confirmation that data was actually being written. The Data Point button was used to actually denote when data was written for the hotwire segment that was currently underway. This was a necessary function since hotwire calibrations were taken at multiple unit Reynold's numbers and the Data Point allowed for writing hotwire data only when on condition. A different file was written for each hotwire condition, including all calibration conditions and all actual measurement conditions, if multiple were used. By having different buttons to dictate which condition was currently being used along with the Re Goal control, the different files could be automatically named based on the conditions provided when the Data Point button was pressed. The last button provided, labeled Rec, controlled whether the pilot's Re slider was displaying Re_c or Del KTAS. Directly above this control was a true/false check box

for Acquire Audio. There was capability built into the LabVIEW program to acquire all in-flight communication which was input into the laptop microphone jack. This feature was not actively used but was more of a legacy feature previously used.

Directly under the Acquisition Parameters section was the Pilot Display Controls section which provided controls for different parts of the pilot display. Controls were provided to control the maximum and minimum temperature of the pilot temperature display along with a control for the center value of the pilot Beta Angle slider. The other control in this section defined the file name for the climb file used to plot the temperature profile during the climb. Both the pilot display and the FTE display provided a readout of temperature, and during the dive this plot provided the temperature profile obtained during the climb as well as a trace of the temperature during the dive. The FTE temperature display was located directly below the Pilot Display Controls section.

The Plasma Configuration section provided a display of measured values to monitor and record the conditions of a plasma system in use at times on the aircraft. Signals were acquired using a Tektronix TDS2014C oscilloscope and then read by LabVIEW. Indicators are provided in this section for the 0-Peak voltage, RMS voltage, frequency, and current of the plasma system. Also provided was a true/false checkbox to turn on or off the ability to acquire the data and an indicator light was provided next to the checkbox to confirm the functionality.

Hotwire was the final section in the FTE display. This section contained four indicators to provide the mean value for the unfiltered signal from each anemometer

channel. By having this displayed on the FTE display the voltage could be monitored to ensure they remain within range, as well as make sure they did not start acting erratically. There was the capability to monitor the output voltage from the anemometer using its digital readout but only one channel at a time, but this required the FTE to look away from the computer. Also included was a control to set the frequency at which the hotwires were acquired. Lastly there was a true/false check box to control whether the functionality to acquire hotwire data was turned on or off along with an indicator light to confirm this functionality decision.

As was noted in the Pilot Display Controls section, the FTE had some form of control on many of the pilot display indicators. The initial version of the displays received by the author had no built in ability to control any of the of the pilot display indicators. Both the Rec and Beta Angle slider had fixed ranges manually defined and never changed. The first time changes were made to any indicators came with changing the scaling of the Beta Angle slider. During this initial change in scaling, the scaling was set manually by the FTE during flight which required stopping the LabVIEW program in order to change the scaling. This was not extremely troublesome if the same β was used for an entire research dive, but if a sweep of multiple β points was performed this became cumbersome. The functionality to set the maximum and minimum values for the Beta Angle slider was then built into the LabVIEW vi. By adding this functionality, the scale of the Beta Angle slider could be changed on the fly with the program running. However, this required changing two different controls each time a change was made in β conditions, but it did allow for easily adjusting the overall scale of the slider. It was

decided by the pilot that a ±1° scale centered at the desired β angle would be sufficient; therefore, the two controls were replaced with one to define the center of the Beta Angle slider and the 1° was added and subtracted to define the maximum and minimum, respectively. A similar technique was used to control the Re slider using the Re Goal control. Except, for the Re slider a scaling of ±0.2x10^6 was used when displaying Re_c and ±2 knots when displaying Del KTAS.

Just as a point of comparison and definition of the FTE display's starting point, the original condition of the FTE display is shown in Fig. 11. This configuration allowed for the acquisition of variables associated with measuring shear stress using calibrated hotfilms as was performed by Woodruff [18]. The current author was not performing calibrated hotfilm measurements, so all of the functionality for calibrated hotfilms was removed from the LabVIEW code in order to allow room for other indicators on the front panel but also free up processor time by not acquiring unneeded data. This was done prior to all of the additions and modification listed above.

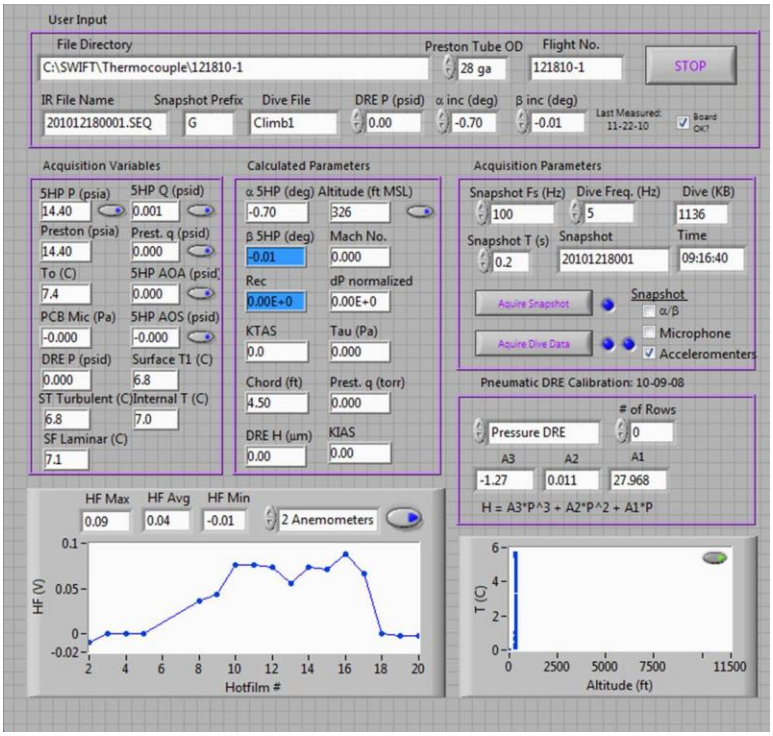

Fig. 11 Original condition of FTE display.

CHAPTER III

PLASMA DRES

The next step in furthering the work performed by previous researchers in the areas of both applique and pneumatic DREs is to find a light, effective, easily installed, reliable replacement. While applique have been shown to be effective and light, they are by no means easily installed as they are applied almost individually across the span of the airfoil. They also must be inspected in detail after installation and repairs must be made to replace DREs that did not go on properly or were damaged. Pneumatic DREs while more easily installed than applique DREs, they were not very effective in flight [5] and the system to control them is not light as it requires a compressed air system along with pneumatic lines. One potential replacement is plasma DREs. Plasma actuators are very light, only require running electrical lines to them, and require only an electrical power system to operate them.

Aircraft Installation

A number of experiments have been undertaken to further the knowledge of LFC on a swept wing along with the intensities of freestream turbulence in-flight. All research was performed at the Texas A&M Flight Research Laboratory. The platform used for these experiments was a Cessna O-2A Skymaster, shown in Fig. 12. All of the stability experiments were performed on the test airfoil model SWIFT, as shown in Fig. 13.

Fig. 12 Texas A&M Flight Research Lab's Cessna O-2A.

Fig. 13 SWIFT in flight with solid, polished leading edge.

A main component needed to complete this work was a power system to run the plasma actuators. The chosen system's base components consist of a HP 33120A function generator, QSC PL380 amplifier, Corona Magnetics resonant transformer, and a Tektronix TDS2014C oscilloscope. Also used are a Tektronix P6015A high-voltage probe and Pearson Model 2100 current monitor that are fed into the oscilloscope to monitor their respective outputs. There were multiple concerns with installing a system running at such a high voltage (~5kV) and frequency (~5kHz) into an airplane, including: electromagnetic interference (EMI), getting the power to the model, and shutting down the system upon actuator failure/burnout. All of these concerns stemmed from the number one concern of the flight lab, and that is the safety of the crew in the aircraft.

The first major hurdle was how to get the power from the cabin of the aircraft, through the wing, and into the SWIFT model's leading edge. It was decided to run the wiring through the leading edge of the wing. This was the location of other wiring for the airplane and instrumentation, as well as the control lines for the control surfaces. By installing the wiring in this location, it was inside of the wing and not outside creating additional drag on the aircraft, nor was the wiring exposed to large amounts of aerodynamic forces. Also, with the wiring installed in the leading edge, the spar separates the wiring from the fuel tanks inside of the wing. The wiring was then passed out of the wing through a hole cut into one of the inspection port panels on the wing. Then the wiring passed through the SWIFT model body into the leading edge. A custom

Teflon block, shown in Fig. 14, was fabricated in order to insulate the connectors inside of the leading from both the leading edge and each other.

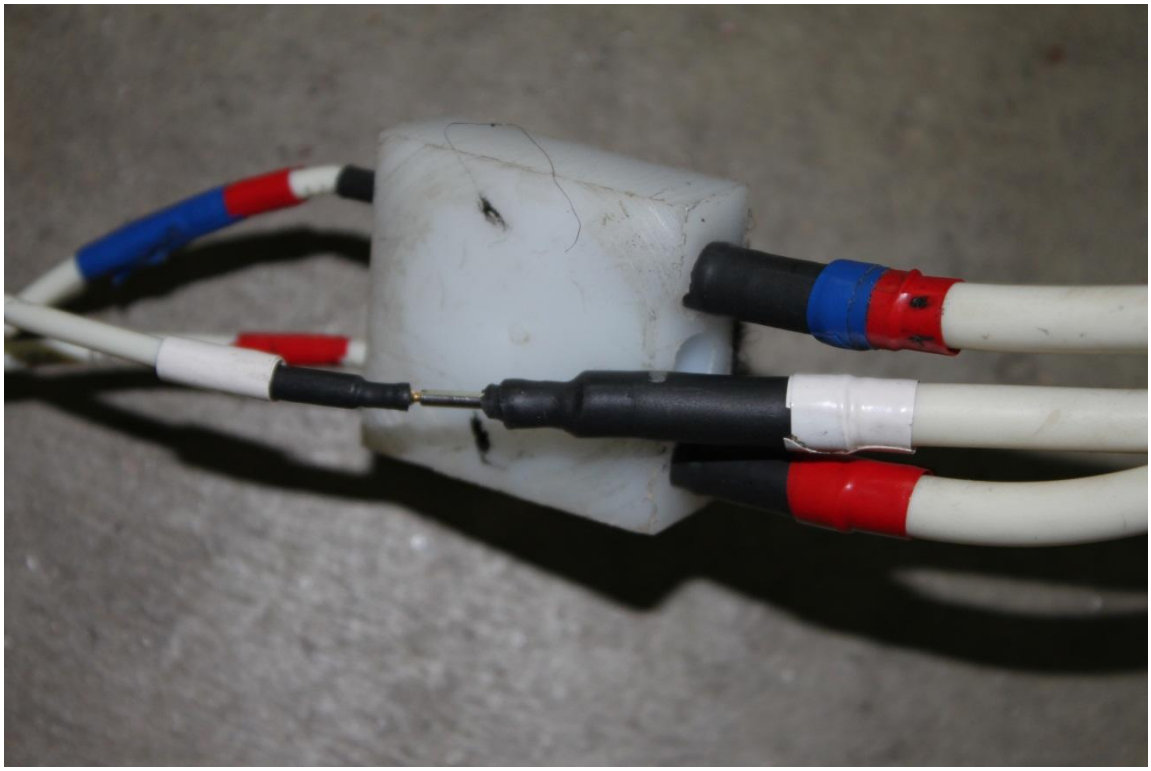

Fig. 14 Teflon connector block for inside of SWIFT leading edge. Middle wire is outside of the connector block in order to show connectors inside of the block.

Electromagnetic Interference

Another major concern was the possibility of EMI from the plasma system interfering with the aircraft radios. The plasma system was only used in flight during the dive portion of the flight, the most critical part of the flight. During this portion of the flight, the pilot was looking at all of the aircraft instrumentation to fly the plane and hold conditions and the FTE was watching the computer and running all of the experimental

instrumentation. This left only the front seat safety observer looking outside of the airplane while we were diving down through vertical airspace at high speeds. An aid to look for other aircraft in our flight path was obtaining flight following from air traffic control, but in order to hear them call to tell of traffic in our flight path the pilot had to be able to hear the radios.

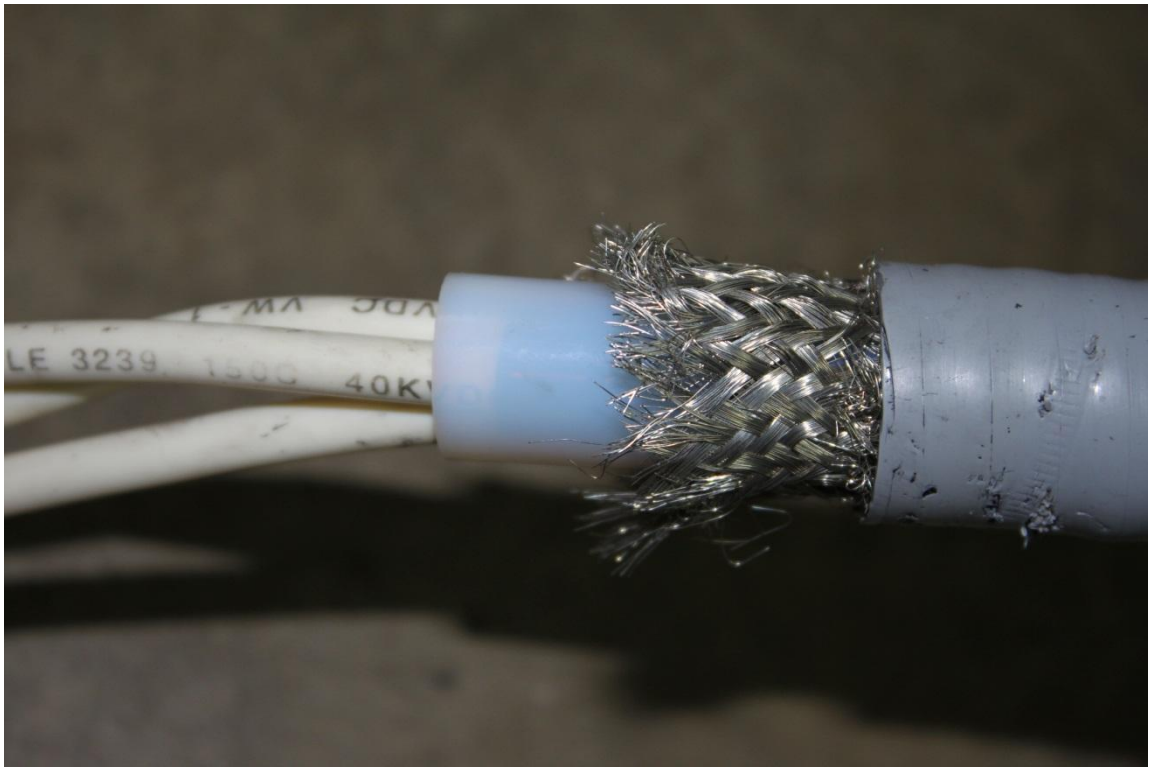

Fig. 15 Plasma wire bundle.

In order to negate any EMI from the plasma system a wiring bundle was built along with a custom enclosure to house all of the power system. Multiple iterations were performed for the wire bundle but the final design consisted of the following components listed in order from inside to out: three-wire “twisted-pair”, Teflon tubing,

wire braid, and conduit, shown in Fig. 15. This bundle not only provided EMI protection, but also provided protection for the high voltage wiring itself as it passed through the wing and the model. It was also found that by placing the entire power system in a metal container inside the airplane significantly reduced the amount of EMI. A custom aluminum enclosure was fabricated in order to house all of the power system, shown in Fig. 16. This box was fully enclosed causing it to act as a faraday cage. It also provided an easy solution to installing all of the equipment into the airplane in a way that was secure but also easily removed in a matter of minutes if necessary.

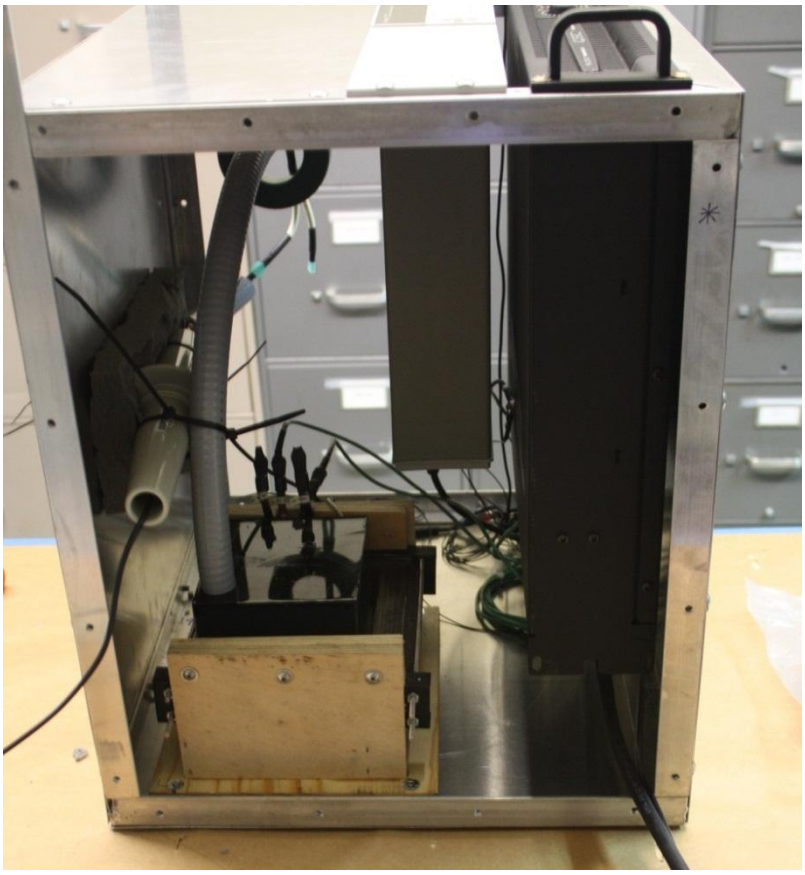

Fig. 16 Plasma power system box and components. The sides were removed to show the interior components.

These solutions helped ease the EMI experienced during ground testing. However, it did not negate all EMI during ground testing. Therefore, testing was performed to determine the levels at which the EMI on the radios rendered the radios unusable and this was set as the limit for flight testing. It was by coincidence that these limits were over 8kV which would become a limit due to actuator burnout as described later. Ground tests were not enough to qualify the system safe for flight. The first time the actuators were turned on in flight was while the aircraft was in the airport pattern to allow for the fastest possible landing in the event of an emergency. No issues arose during this test, and the EMI experienced in flight, during this test or at any time during the project, was never as high as that experienced on the ground.

Emergency Cutoff

The last major area of concern with the plasma system was a way to shut the entire system off automatically in the event of a burnout of the plasma actuator, or even a short in the wires. An initial design involved measuring the impedance of the signal going into the plasma actuator and looking for a drop in the impedance. This design did work, was automatically controlled via LabVIEW, and cut power to both the power amplifier and the function generator. However, there was a significant lag in the system, on the order of at least two seconds, and this was deemed unacceptable. A couple of factors added together to cause this lag in shutoff. The voltage probe used would not work directly with the DAQ boards installed in the aircraft, but was made for use with a Tektronix oscilloscope. At first glance this was not a significant issue because the oscilloscope's signal could be relatively easily fed into LabVIEW. However, the oscilloscope's signal

was not read by LabVIEW as a continuous stream of data but rather as a snapshot of data. This led to a lag between when the measurement actually occured and when LabVIEW actually received the data. A lag also exists between the time LabVIEW received the data, had actually calculated the impedance, and a signal was received by the cutoff box to shutoff. Therefore, a new method was needed to shut the system off that did not involve LabVIEW.

A new design was conceived that relied on a fuse on the power line running into the power amplifier and function generator. There was a high enough increase in current draw on the AC power lines powering the system upon actuator burnout that a fuse would blow upon burnout of an actuator. This new system removed power from the power amplifier and function generator in under half a second, and was employed in all plasma testing.

Plasma Insert

In order to install the plasma actuators onto SWIFT a new leading edge insert was designed and fabricated for the plasma actuators. The new design was a two-part design consisting of an aluminum outer portion that was used for all of the plasma inserts along with an inner-portion made out of G-10 garolite which holds the plasma actuator. The two pieces of the insert can be seen installed in the leading edge in Fig. 17, but the garolite insert does not have a plasma actuator installed on it. One major disadvantage to the current setup was the amount of time required to install each actuator. Each actuator requires its own garolite insert which was sanded and prepared to flight standards. This was a labor intensive and time consuming process, and was one reason for going with

the two piece insert design. The two pieces allowed for a reduction in the material needed for each insert, as well as reducing the amount of material that needed sanding.

Fig. 17 Blank garolite insert with aluminum outer insert installed in leading edge.

A process was formed to produce the inserts and get them to flight quality standards. The inserts were first machined with the final cut on the top surface being made in 0.0005in steps with a 0.5in ball end mill in order to give the smoothest finish possible. The insert was then sanded going from 600 grit up to 3600 grit sandpaper. After the initial sanding the insert was sent back to the machine shop where a slot was cut for the plasma actuator. For each individual actuator a custom slot was machined according to that actuator's dimensions. This provided the best possible fit for the actuator. Next nylon screws were installed into the actuator and formed a rest for the actuator that can be adjusted in order to get the best alignment possible between the actuator and garolite insert. RTV silicon was used to glue the actuators onto the garolite, and the insert was installed into a mold containing a Teflon reverse blank of the insert. After the silicon was cured, the insert was sanded prior to installation on SWIFT. The junction between the actuator was sanded up to 2mm onto the actuator in order to remove any steps in the junction. Once again the sanding went from 600 grit up to 3600 grit. The insert was then

installed and shimmed to fit. This process was extremely time consuming and was not feasible for any type of commercial application. Also this process introduced too much deformation into the shape of the insert which made it extremely difficult to get a proper fit on the model and not get any turbulent wedges coming from the insert. A fabrication process that actually builds the plasma actuator into the insert is desperately needed.

Leading Edge Tape

Plasma DREs were ineffective on a polished leading edge so it was desired to increase the surface roughness on the leading edge in order to destabilize the crossflow disturbance and possibly provide better conditions for the plasma actuators to work with. In previous studies with the SWIFT model and applique DREs the leading edge was painted [5]. However, a solution was desired that did not involve the removal and painting of the leading edge. It was also believed that it would be sufficient to only increase the roughness upstream of the plasma actuators.

A solution to this was solved by applying spray paint to Kapton tape. Kapton tape was chosen because its surface was extremely smooth and it does not leave a residue when removed and therefore it would not have any adverse effects on the leading edge when removed. The Kapton tape was pulled out and suspended between two wood blocks. Spray paint was then applied and allowed to dry for a few minutes before the tape was applied to the leading edge. This method removed the need to somehow cover the SWIFT model to protect it from any overspray from the spray paint. The installation of the spray painted tape is shown in Fig. 18.

Fig. 18 Spray painted tape applied to leading edge.

It was also necessary to determine the roughness of the spray painted tape in order to compare it to that of the polished leading edge. Measuring the roughness of the tape installed on the leading edge was not possible without removing the leading edge; therefore an alternative solution was devised. A test piece of aluminum was sanded and

polished to a roughness of RMS = 0.057 μm, equivalent to the polished leading edge, and a sample piece of tape was spray painted and applied. The roughness of the spray painted tape was RMS = 1.21 μm. This result revealed that the spray painted tape would increase the roughness upstream of the actuator and was close to the value previously employed by Carpenter [5]. However, with all of this work, plasma actuators were still ineffective at delaying transition.

Hotfilms

Due to the ineffectiveness of the plasma DREs, along with the unsteadiness of the actuators as demonstrated by Craig et. al [19], a theory arose that instead of controlling the stationary crossflow waves on the airfoil the plasma actuators may have been exciting a travelling wave on the model and causing early transition. In order to determine if a travelling wave was present, a Tao Systems Senflex 93021 hotfilm was installed on the model as shown in Fig. 19.

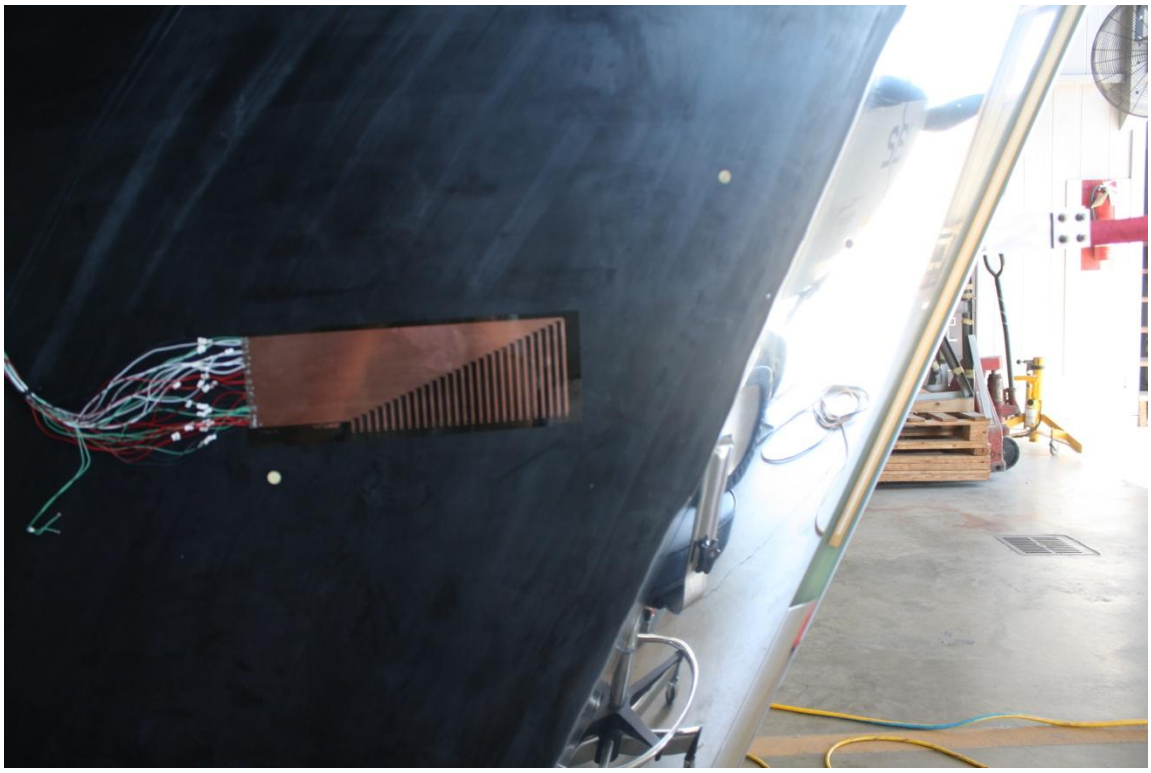

Fig. 19 Installation of hotfilm on SWIFT model.

Power spectral density (PSD) analyses could then be performed on the signals from the hotfilm sensors to determine if a travelling wave is present by comparing the signal with the plasma actuators off versus with the plasma actuators on. Any frequency spikes noticed after the plasma actuators were turned on would be the result of some effect from the plasma actuators. It was found that no travelling wave was present due to the plasma actuators as no change was seen in the PSDs between plasma on and plasma off, as shown in Fig. 20.

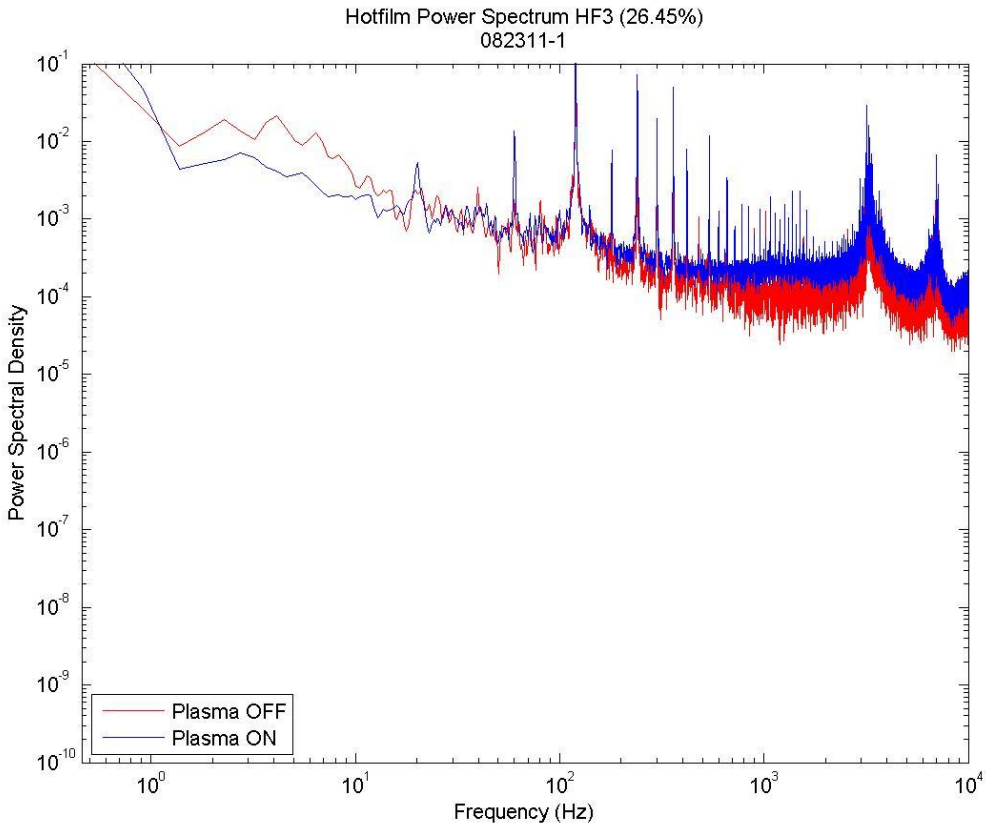

Fig. 20 Hotfilm power spectral density showing no travelling wave.

Painted Leading Edge

With the ineffectiveness of the spray painted tape applied around the leading edge and the determination that no travelling wave was present it was determined that the only logical next step was to remove the leading edge and paint it. Jet Glo conventional 570 series urethane paint in Matterhorn White, with no primer or thinner, was applied to the leading edge to increase the surface roughness as was previously employed by Carpenter [5]. The leading edge and both parts of the insert were all painted separately and then later reassembled. Figure 21 shows the final assembly of the painted leading edge and

plasma insert. This paint job resulted in an RMS roughness of 2.42μm and an average peak-to-peak of 12.17μm. Even with painting the entire leading edge, plasma DREs were still ineffective at controlling the transition location.

Fig. 21 Painted leading edge with plasma insert.

Conditions Run

In an effort to show the effectiveness of plasma DREs at delaying transition, multiple configurations were used ranging from different aperture shapes to varying the voltage and frequency of the input signal. The most significant change tried was the different actuator shapes that were tried to get the plasma DREs to work. Figure 22 shows three of the different actuators used. The left most picture is 1mm diameter, the center is 1x4mm rectangles, and the right most picture is line actuators. All of the apertures were spaced at 2.25mm. Also used but not pictured were 1.5mm diameter circles spaced at 2.25mm and 3mm circles spaced at 6mm. While the goal of plasma actuators was to extend laminar flow, these actuators were designed to provide wavelength control to where either all or every other aperture could be turned on. By turning every other aperture one an unstable wavelength could be excited and move transition forward. At first this may sound like backwards progress, but by demonstrating the ability to move transition forward the installation and ability of the actuators could be validated. This was the goal of installing the 3mm diameter apertures spaced at 6mm, as 6mm is an unstable wavelength on this platform. However, at no point were the plasma actuators successful at moving transition forward.

Fig. 22 Plasma actuators used in-flight. Left: 1mm diameter. Center: 1x4mm rectangles. Right: line actuators.

Lessons Learned

Even though success has yet to be achieved with plasma actuators, many lessons have been learned throughout the process that will help future researchers in their work with plasma actuators. The first of these lessons was that the apertures have to be filled in

order to smooth out the surface. For the actuators used in this work, a hole or step could exist that was as large as 10μm. However, it was found that paint primer could be used to both fill the holes in the apertures and in the case of the line actuators, level out the surface and remove any steps associated with the electrodes. The primer could also be sanded to provide a smooth surface.

Another issue that arose came from the use of the wavelength control previously mentioned with the plasma actuators. Due to the design of the SWIFT airfoil, the control wavelength was 2.25mm hence making the plasma apertures 2.25mm apart. However, due to the nominal size of 1mm diameter for the apertures, each buried electrode was only 1.75mm from its adjacent aperture. It was discovered that if the 4.5mm wavelength was used, meaning every other aperture was on, after a period of use arcing would start occurring between the active electrodes and the inactive electrodes. This was believed to be caused by either a breakdown of the RTV silicon used to assemble the actuators and inserts or an air bubble trapped in the silicon. While the inactive electrodes were not grounded, they were not hooked to anything, the electrical potential between the inactive and active electrodes, nominally 5000V, would make the inactive electrodes act as if grounded. Two solutions were determined for this issue. First, the actuators could continue to be used safely as long as all of the apertures were activated and not just every other one. This removes any electric potential between any of the buried electrodes and completely negates the issue. Second, it was determined that the issue could also be solved by applying a small layer of Super Corona Dope to the actuators prior to assembly. Super Corona Dope is a liquid that flows more freely and allows for

removal of all air bubbles as well as having a dielectric strength of 4100kV/in compared to approximately 550kV/in for RTV Silicon.

It was also learned that extreme care has to be used when soldering leads onto the buried electrodes. Care had to be taken to not have any sharp points on the solder as this could cause burnouts on the actuators. Also, if too much heat was used when soldering the leads to the electrode the dielectric material could be damaged leading to a burnout that actually burns through the actuator at the point of the junction, as shown in Fig. 23. The only way known to effectively solve this issue was to take care while soldering the leads to the buried electrode and to limit the voltage applied to the actuators. After this burnout type was detected, the voltage on the actuators used in flight was limited to 8kV as it took approximately 9kV before this type of burnout would occur.

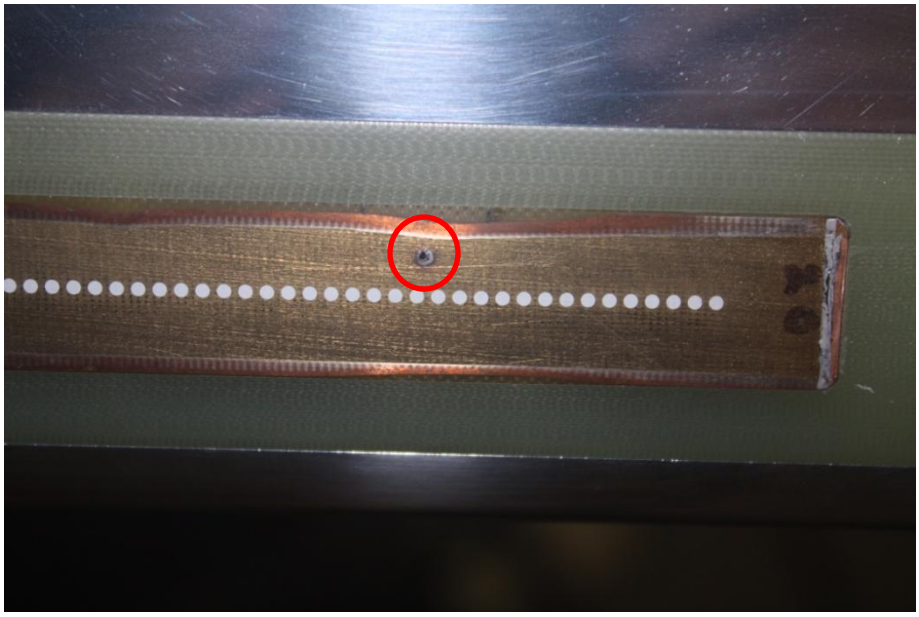

Fig. 23 Actuator burnout due to dielectric damage from soldering.

The last significant lesson learned involves prepping the actuator for a painted leading edge setup. In the condition that was flown, an existing plasma insert was painted and installed in the leading edge. There were multiple issues with this. One, the paint was applied without the use of primer which increased the chance that the paint would chip. A solution to this was to install the insert and paint the leading edge and insert as one piece. Another issue was that the actuator was sanded flush with the insert, but was then masked off for painting. Since the actuator was not painted, two steps were induced, both before and after the actuator. One solution that was tested to solve this issue was to paint over the actuator. A test actuator was painted and seeding particles were placed on top of the actuator. It had already been shown in some previous testing with these actuators that the force from the plasma actuators would move the seeding particles once the actuator was turned on. However, with the actuator fully painted the seeding particles were not displaced. This resulted in there being no force from the plasma actuators, rendering them useless. It should be noted that painting an actuator is different from applying the filler previously mentioned. The filler only covered the dielectric material exposed by openings in the exposed electrode; whereas painting the actuator actually covered the exposed electrode. A solution was later determined, but never tested or implemented, to install an actuator onto an insert with the intention of painting it so that the actuator is installed slightly raised above the insert. This allows for masking the actuator and painting the insert, but when the mask is removed the actuator and paint on the insert should be roughly flush.

Conclusions

Plasma DREs have yet to be shown to stabilize the boundary layer and thus delay transition. However, it has also not been proven that the plasma DREs experimental setup is in a condition to allow for boundary layer stability. There is still hope for plasma DREs to work given the recent success of Schuele in a Mach 3.5 flow [11]

CHAPTER IV

APPLIQUE DRES

Since success with plasma DREs was not achieved, it was desired to be able to say with certainty that plasma DREs were ineffective at delaying transition and that the issue was not with the experimental setup. The only real way to do this was to go back to a tried and tested method that if it worked under the same conditions as plasma DREs then it could be definitively stated the plasma DREs do not work. This method was applique DREs. Applique DREs were the method previously used by Carpenter to delay transition on the SWIFT model in flight [5].

Plasma Inserts

Rather than go back to the inserts used by Carpenter, it was desired to show that applique DREs worked in conjunction with the plasma inserts in order to deem the experimental setup valid. However, the DREs could not be applied directly over the plasma actuators. As mentioned previously, a filler was applied to the plasma actuators to level the surface of the actuators and remove any steps, gaps, or holes on the actuators. This filler was not resistant to either ethanol or acetone, one of which is needed to remove DREs once applied. Therefore, the applique DREs were applied upstream of the plasma actuators. Applique DREs were installed on many different test configurations of the plasma DREs, but they were first applied during the trials with the spray painted Kapton tape applied around the leading edge as can be seen in Fig. 24. In

this configuration, 1mm diameter circular applique DREs were applied at 0.7% chord at a wavelength of 2.5mm. Roughness heights of 6, 12, 18, and 24 μm were also used. None of these configurations proved effective.

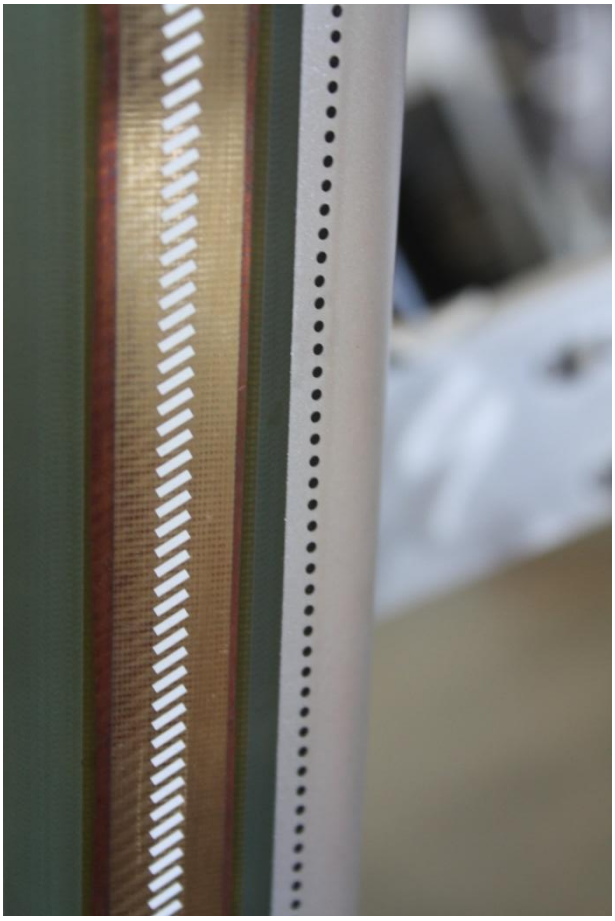

Fig. 24 Applique DREs applied on spray painted Kapton tape.

Applique DREs were also applied to the painted leading edge as seen in Fig. 25. This time the DREs were applied at 1% chord, just upstream of the plasma actuator. The same 1mm diameter circular applique DREs spaced at 2.5mm were used with roughness

heights of 6, 12, and 18 μm. There configurations were also deemed ineffective at delaying transition.

Fig. 25 Applique DREs on painted insert leading edge.

Solid Leading Edge

Due to the ineffectiveness of both plasma and applique DREs used in conjunction with the plasma inserts, it was decided to change leading edges to a solid one that did not have a cut out for an insert. This would remove any surface discontinuities resulting from the insert installation and provide the best possible platform for testing DREs. Multiple paint jobs were tried on the solid leading edge, using the same paint treatment as described before. All resulted in different roughness levels.

The first paint job was the condition in which the solid leading edge was already. It had been used previously to test the effectiveness of a polishing agent, called Granitize, to extend laminar flow over an airfoil by reducing the roughness of a painted surface. This paint job had an RMS roughness of 0.84μm and an average peak-to-peak of 4.0μm measured at 3% chord. This surface finish was only slightly higher than that of the polished leading edge, but also did not have the orange peel texture described by Carpenter that has been proven effective in the past when used with DREs [5]. Applique DREs with a 1mm diameter were spaced at 2.25mm along 1% chord with roughness heights of 10 and 20μm. No success was achieved with this leading edge finish, so it was decided to strip the leading edge and repaint it.

The same paint technique was used to achieve a paint job with an RMS roughness of 2.5μm and an average peak-to-peak of 11μm measured at 2% chord. This provided both the desired orange peel texture and a roughness significantly higher than the polished leading edge. On this configuration, 1mm diameter DREs were spaced 2.25mm apart at roughness heights of 10, 20, and 30μm tried at both 0.6% and 2% chord, individually.

The same configuration was tried at 1% chord with a roughness height of 10μm. Success was still not achieved, so it was desired to try reducing the roughness on the leading edge.

In order to reduce the roughness of the leading edge, the first 5% chord was sanded with 1500, 2400, and 3600 grit sandpaper. The roughness was subsequently reduced down to an RMS of 1.52μm and an average peak-to-peak of 6.43μm measured at 2.1% chord. Multiple applique configurations were then tried on the paint job. First was 1mm diameter DREs spaced at 2.25mm at 1% chord with roughness heights of 10, 20, and 30μm. Followed by 1mm diameter DREs spaced at 2.75mm at 1% chord with a roughness height of 11μm. The same configuration was applied at 2% chord with heights of 11 and 22μm. 1mm diameter DREs placed along a line running from 0.6% chord at the root pressure port row to 0.66% chord at the tip pressure port row, with a height of 11μm were also tried. The final configuration tried with this paint job was 1x2mm oblong DREs spaced at 2.75mm with a roughness height of 11μm applied at 0.63% and 1.1% chord, individually. The oblong DREs were applied in such a way that the 1mm side was perpendicular to the flow and the 2mm side was parallel. Success was still not achieved with any of these configurations so it was decided to see how the DREs would work on a solid polished leading edge.

All of the paint was stripped from the leading edge. The leading edge was then sanded and polished down to a surface finish similar to that on the leading edge used with the plasma inserts. Roughness measurements were taken at 0%, 0.6%, 1%, and 2% chord with a RMS roughness between 0.30-0.41μm and an average peak-to-peak between

1.95-2.34μm. This provided an adequate finish to perform measurements on a polished surface. Applique DREs 1mm in diameter spaced at 2.5mm with a roughness height of 11μm were applied at 1% chord, but they also did not work. The work is ongoing through researchers that have taken over the project, but the problem has not been solved.

Lessons Learned

There were a few lessons learned through all of this work that could help future researchers in their endeavors. First, was how to align the applique DREs for installation. The first technique employed, which was a pass down from previous researchers, was to use a laser level on a tripod on the floor of the hangar. Many issues arose from this setup. First, with this setup the laser level was not kept in rigid alignment with the model which meant that it could easily have been bumped and moved out of alignment because it was typically in close proximity to whoever was applying the DREs. Also, the airplane, and subsequently the model, was able to move independently of the laser level so if anyone else was working in or on the airplane the model would move around and might not have settled back to the same exact position. Second was that the width of the laser line was not constant. It is known that laser beams do not have a constant diameter, but contract down to the beam's waist and then diverge again. This most likely was one of the factors in why the laser level's line was not constant width. The main issue with this non-constant width was determining where to align the DREs relative to laser line (i.e. center or edge of the line). Therefore, a solution was desired to improve on these conditions

The second technique used was a piece of string that was stretched along the chord location of interest and taped in place. This technique was much of an improvement over the laser line because the string was directly attached to the model so that it cannot move independently of the model. Also, the string's line could not be blocked as the laser line could be if the person putting on the DREs got in the path of the laser. Aligning the string was also much easier as fine adjustments were very easy to make. With the string adjustments could be made on each end of the string to get it aligned perfectly at the desired chord location. Whereas, with the laser there is a constant beam so that the entire beam has to be rotated and then moved to the chord line to align it. The string also offered a more constant width than the laser line; however, it was not exactly constant as there were small bumps, threads, and other features on the string that caused some issues, as can be seen in Fig. 26. Determining where to align the DREs relative to the string was not an issue though as the back edge of the DREs could easily be aligned with the edge of the DREs. Care was taken to place the edge of the string one radius of a DRE off of the desired chord line so that the centers of the DREs were placed along the chord of interest. Even with the great advantages of the string over the laser line, there were still disadvantages such as the still not quite constant line and the threads hanging off the string that could get caught under the DRE requiring their replacement.

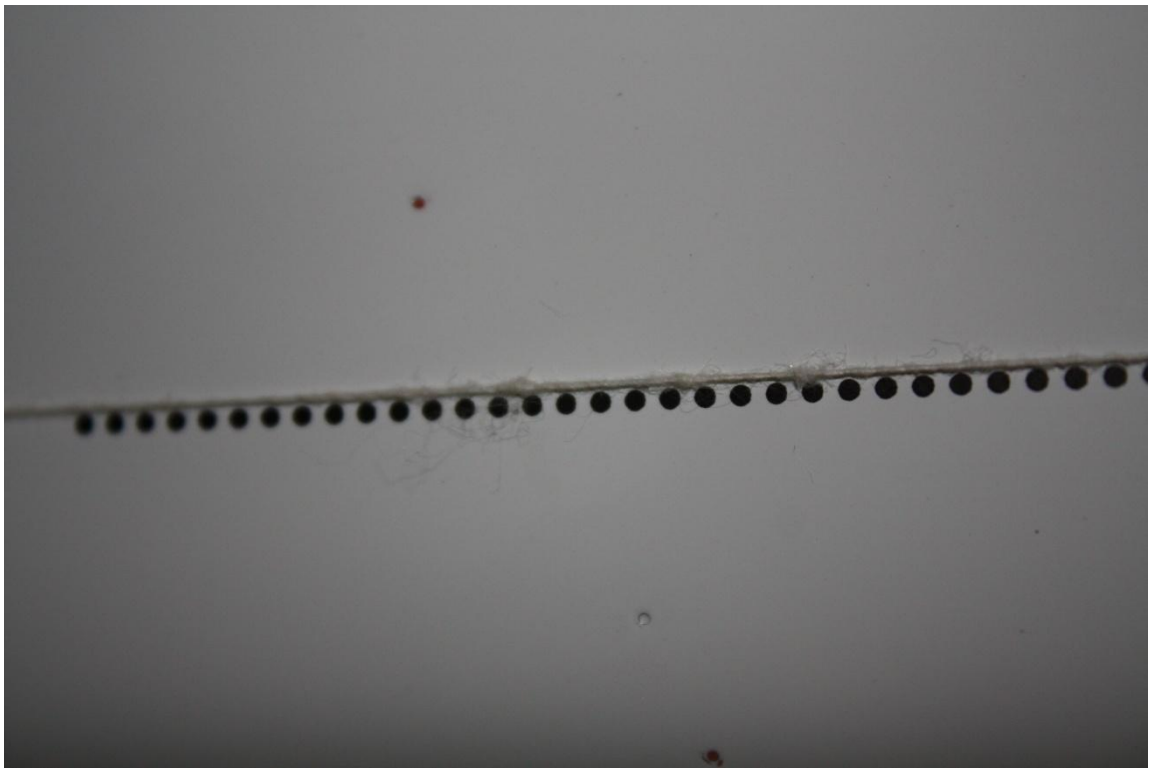

Fig. 26 String used to align applique DREs during application.

The third technique used to align DREs was monofilament fishing line. Monofilament fishing line solved the remainder of the issues. Since it was a monofilament there were no treads to get entrapped under the DREs nor any bumps in the line, meaning that it was a constant diameter its entire length. Also of unknown advantage until it was used was that the monofilament could be purchased in different colors allowing for a very pronounced color contrast, as seen in Fig. 27. The only remaining disadvantage was that the sheets containing the DREs had to be slipped under the string during application in order to get the DREs aligned and installed. This disadvantage was far outweighed by the advantages offered by the monofilament fishing line.

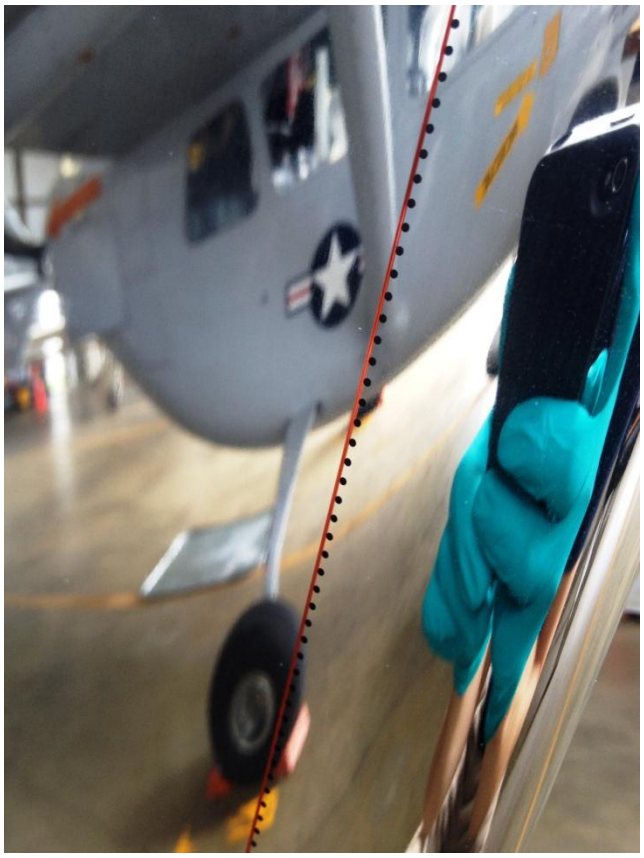

Fig. 27 Monofilament fishing line used to align applique DREs.

One other lesson learned through this use of applique DREs was that they do have a shelf life. While the shelf life was not necessarily a constant, the DREs would reach an age where multiple issues arose. One of the issues was that the DREs became brittle and extremely difficult to apply because they would break during application. This drastically increased the amount of time required to apply the DREs as more DREs require removal and replacement during application. Another age issue was that the adhesive on the DREs lost its effectiveness which would cause the DREs to either not

stick to the surface or come off once air flows across them. The only solution to this problem was to purchase new DREs.

Conclusions

While success has not been achieved with applique DREs during this round of testing some useful knowledge has been attained through the process. Applique DREs have not been shown to work in situations where plasma DREs have not. This renders hope that plasma DREs can eventually be shown to be an effective solution for laminar flow. Better techniques have been developed to align and apply applique DREs than were previously used. It was also determined that DREs do not have an infinite shelf life but rather reach a point where they must be replaced.

CHAPTER V

HOTWIRES

Experimental Setup

One lingering question throughout the entire SWIFT program has been what are the true turbulence levels in flight? But also how do turbulence levels change with different seasons of the year? In order to determine this, hotwires had to be reinstalled onto the aircraft in order to measure the freestream turbulence levels in flight. A hotwire sting mount, first used by Carpenter, already existed for use on the aircraft [5]. Since then, it had been being used as a counter weight to help offset the moment arm of SWIFT. This sting mount was already equipped with probe supports to hold 4 single wires; however, it was desired to perform temporal correlations on the hotwire signals in order to remove both electronic noise and acoustic sound. The sting mount was modified to hold dual wire probe supports in both the top and bottom positions. Dantec 55P71 parallel array hotwire probes were installed in both the bottom and top probe supports, which are a distance of 12in apart, as seen in Fig. 28. These probes are designed with two parallel wires space 0.4mm apart allowing for simultaneous measurement of small scale turbulence. This setup was effective because the turbulent length scales that are important to receptivity research are O(1mm) because they have to fit inside the boundary layer. Carpenter showed that SWIFT's boundary layer height was approximately 0.5mm at 7% chord and 1mm at 35% chord, both at -4.69° angle of attack

[5]. Since the two wires on each array were only 0.4mm apart, both wires would sample turbulence with a length scale greater the 0.4mm. Since the probes were spaced 12in apart, their distance was significantly larger than the turbulence length scales of interest, but would still acquire any acoustic sound over both probes. It should be noted that while referred to as acoustic sound, temporal correlations removed any part of the signal that showed up across the wires spaced a distance apart. This removal could include unsteadiness in aircraft velocity that presented itself on the measurements or even aircraft vibrations such as was seen by Riedel and Sitzmann [16]. For the sake of simplicity all of these phenomena will be lumped under the heading of acoustic sound.

Fig. 28 Hotwire sting mount in flight with two dual-wire probes installed.

Also, an anemometer and bandpass filter had to be installed into the aircraft in order to run the hotwire. One complication was the size of the anemometer - AA Lab AN-1003 anemometers weigh 50lbf. At the time of installation, other equipment was installed in the location on the cabin floor behind the pilot previously used for installing the anemometers. The only place left within the cabin of the aircraft for the installation of the anemometer was the top of the instrumentation rack. It was determined that this installation location would not push the aircraft's center of gravity past its aft limit. However, its installation did severely limit the fuel available for the flight. If both the anemometer and plasma box were installed, the flights were run on minimum fuel. A new anemometer bracket was built in order to attach the anemometer to the top of the instrumentation rack. An arresting cable was installed around the anemometer and attached to the shoulder harness connection point on the aft firewall in order to keep the anemometer securely in place in case of a high forward g-loading, such as would be encountered in the event of a nose-wheel collapse. A Kronhite Model 3016 bandpass filter from 1Hz – 15kHz was used to filter the hotwire data prior to acquisition. The installation of the hotwire instrumentation and plasma equipment is shown in Fig. 29.

Fig. 29 Rear of O-2 cabin with hotwire and plasma instrumentation installed.

In order to properly tune the hotwires on the anemometer, the existing wiring on the aircraft running to the sting mount was replaced. The existing wiring in the starboard wing connecting to the sting mount and hotwires was RG-174/U coaxial cable; however the AN-1003 anemometer channels are tuned for specific lengths of specific wiring types. The channels in use on the aircraft were tuned for 5m lengths of RG-58. Due to this discrepancy, the hotwires were unable to be tuned effectively and the wiring required replacement. In addition to replacing all of the wiring, all of the connectors used on the wiring were replaced as well. Existing on the aircraft were two CPC circular connectors, one in the cabin and one on the wing. These connectors have the disadvantage that they require the coaxial cable's inner wire and shielding to be split off

to go through pin connectors. Having two connection points increased the potential for signal reduction. Because of this, the connector in the aircraft cabin was completely removed with the wires running straight from the anemometer out the aircraft wing. The connector on the wing was removed and replaced with individual BNC connectors on each wire. These connections could not be removed because they are necessary to allow the removal of the sting mount.

Theory

All of the hotwire data, both filtered and unfiltered, along with all air data was acquired at 45kHz using LabVIEW and written directly into a binary file. After the flight, the file was imported into MATLAB and the freestream turbulence intensities were calculated using the technique described by White [20] with a couple of modifications for use in the flight environment. White drew from Bearman [21] who provided that King's Law, Equation (1), could be used to describe the response of the hotwire anemometer as shown in Equation (2).

$$Nu = A + BR_e^{\frac{1}{2}} \tag{1}$$

$$E^2 = k(T_w - T_a)A + R_w lk(T_w - T_a)B\left(\frac{\rho U d}{\mu}\right)^{\frac{1}{n}} \tag{2}$$

Bearman then made the assumption that both density and viscosity are relatively constant since they are only slightly dependent on fluid temperature. Therefore, they could be lumped into the constants *A* and *B*. This provided an equation that would be

dependent on velocity and temperature. All of this works for a wind tunnel, but provides a bad assumption for the flight environment. Not only are there temperature variations in the flight environment, but also significant altitude variations. For the current work, hotwire measurements were taken at altitudes differing by as much as 9000ft. Therefore, for this work, unit Reynold's number per meter was used for all calculations, instead of just freestream velocity. This provided Equations (3), (4), and (5), provided by White, for hotwire calibrations modified for the flight environment.

$$C_T(R_e') = \frac{E_h^2 - E_l^2}{T_h - T_l} = -A - B\ R_e'^{\frac{1}{n}} \tag{3}$$

$$E_{comp}^2 = E^2 + C_T(R_e')(T_{comp} - T) \tag{4}$$

$$R_e' = \left[A + BE_{comp}^2\right]^n \tag{5}$$

Where E is the anemometer output, T is the air temperature, T_{comp} is an arbitrary temperature constant, subscript h denotes high temperature, and subscript l denotes low temperature. Calibration points were taken at high altitude to provide the cold calibration data, and then data was taken at low altitudes to provide the hot calibration data. The actual measurements for calculating freestream turbulence were taken at an altitude between the two calibration altitudes.

Experimental Procedure

To get all of the data for the hotwire calibrations and temperature compensation, the standard procedure for research flights established by Carpenter [5] required

modification. During the preflight, the hotwires were installed and the resistance was balanced for all of the hotwire channels on the anemometer and an 80% overheat was applied. It was discovered early on that the damping could not be adjusted prior to flight because right after takeoff the anemometer would go into oscillations. Therefore, a Tektronix TDS2014C oscilloscope was installed in the aircraft cabin in order to tune the hotwires in-flight. During the flight, after passing through 3000ft, each hotwire channel damping was tuned and a gain of 25dB was added. Flights would continue climbing to 12,500ft, instead of 10,500ft, to allow room to perform the cold calibrations without sacrificing altitude for the research dive. Flights would only climb to 12,500ft because 12,500ft is the legal maximum altitude for operating a civil aircraft without pressurization or supplemental oxygen [22]. Upon reaching 12,500ft, the pilots would level off and slow the airplane to 90 KIAS to allow for setting the voltage offset for the hotwires. The offsets were performed at these conditions because for the AN-1003s the output voltage is proportional to altitude and inversely proportional to velocity. Therefore, flying at 90KIAS at 12500ft provides the maximum output voltage that can be seen for the flights. At this point the hotwires are tuned and ready to start the calibration procedure.

In order to perform the calibrations, data was needed for multiple speeds at two different temperatures. The initial method used to fly the aircraft at different speeds was to use the airspeed indicator; however, this method provided some complications during post-processing and turbulence intensity calculations. Using the air data from the five hole probe to calculate indicated air speed that matched the indicated on the aircraft

airspeed indicator was not an easy or trivial process. The five hole probe directly calculated true airspeed via its measurement of dynamic pressure so true airspeed was initially used for all hotwire calculations. This caused issues when performing the calibrations because the difference between indicated airspeed and true airspeed changes with altitude. It was therefore determined that the easiest solution would be to have the pilots fly using true airspeed instead of indicated airspeed. This change allowed direct matching of the calculated velocities at the upper and lower altitudes which was valuable because having velocities close to each other increased the quality of the calibrations. It also meant that there was less of a change needed during the linear interpolation to get an exact match of the velocities which was necessary because the change in output voltage squared for a velocity change of 0.1m/s is equivalent to the change induced by a 5°C temperature change [20]. This method was used until the discovery was made that a Reynolds number should be used for all hotwire calibrations instead of just velocity, as detailed above. Performing all hotwire data acquisition using unit Reynold's number to control the aircraft velocity was the last piece of the puzzle for getting hotwire measurements in-flight.

Since it was determined that *Re'* should be used to control the aircraft velocity during hotwire measurements, the cold calibrations data was collected at *Re'* from 2,700,000 – 4,700,000 1/m in 200,000 1/m increments. Some of the higher *Re'* were not attainable in level flight, so the pilots were allowed to descend as needed to hit the required points. The cold calibrations were started at 12,500ft, but the lowest altitude reached during the cold calibrations was noted so that the actual hotwire measurements could be acquired

below this altitude and above the hot calibration altitude. Upon completing the cold calibrations, the actual hotwire measurements for calculating freestream turbulence intensity were taken, and then the research dive was performed. Hot calibration data was then taken after the research dive, typically between 6000ft and 3000ft. The hot calibrations were performed at the same *Re'* values as the cold calibrations to allow for the temperature compensations.

Going through a range of *Re'* to perform the calibrations caused slight issues for the pilots since they did not have an intuitive feel to how much change in velocity was needed to affect the needed change in Re'. This was remedied by having LabVIEW calculate the true airspeed needed to attain the desired Re' and providing the pilots with a differential between the aircraft's true airspeed and the desired true airspeed on a slider that was centered on zero.

After the flight, all of the data was run through the aforementioned MATLAB code to calibrate the hotwire voltages and calculate the velocity fluctuations. Electronic noise and acoustic sound then needed removal. Naguib lays out a technique for a second-order temporal correlation of two signals that outputs both the correlated and uncorrelated portions of the signal [23]. Also, a code using this technique already existed at the Klebanoff-Saric Wind Tunnel that was written by Robert Downs. In order to remove electronic noise from the signal, the velocity fluctuations for both parallel arrays were put into the filter. The correlated signal between the two wires from each hotwire array contained the velocity measurements and acoustic sound; while the uncorrelated part contained the electronic noise in the signals. The correlated signals from the two arrays

could then be input into the filter to extract the correlated and uncorrelated parts of the two arrays relative to each other. The correlated portion of the two signals contained the acoustic sound, and the uncorrelated part contained only velocity fluctuations due to freestream turbulence. The root mean square of these velocity fluctuations was divided by the mean of the velocity measured by the hotwires to provide the freestream turbulence intensity.

During some flights peaks and erratic behavior were seen in the filtered hotwire voltages along with the unfiltered voltages. The source of this behavior is not exactly known but could be the result of fluctuations in aircraft velocity during hotwire measurements, large scale turbulence, or possibly some issue with the DAQ board. It was desired to know the effect these artifacts have on the hotwire measurements and determine the effectiveness of the correlations to remove them. An example of this situation can be seen in Fig. 30. The signal was very erratic at the beginning of the data set. One option to remove this artifact was to simply truncate the data set and remove it. This had a significant effect on the initial measurements and reduced the average calculated turbulence intensity across all four wires prior to correlations from 0.100% to 0.067% revealing that this was not a trivial artifact. However, it was desired to know what effect would be seen after the correlations were performed. Correlations were performed on both the full and truncated data and calculated a turbulence intensity of 0.023% and 0.021%, respectively. The difference in the turbulence intensity after performing the correlations reveals that the correlations were effective and sufficient to

remove artifacts in the measurements that were on all of the wires and appear unusual, and therefore manually truncating data was unnecessary.

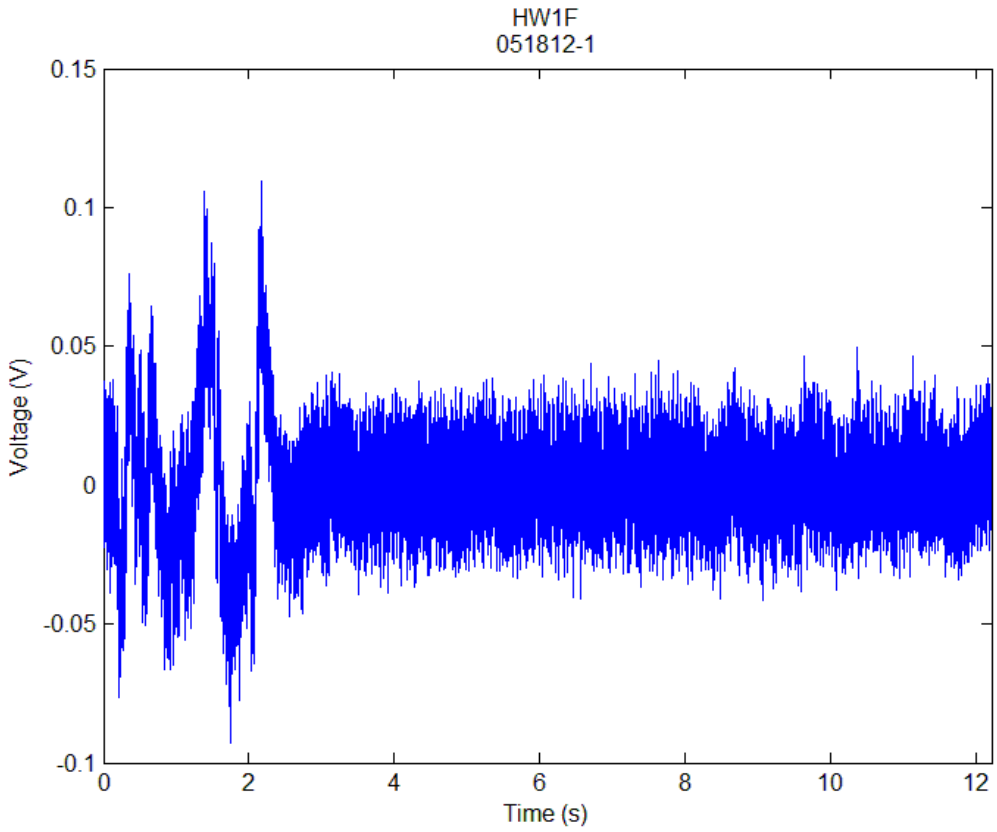

Fig. 30 Raw filtered hotwire voltage with erratic behavior at beginning of sample.

Once the majority of the bugs were worked out of the method for performing straight wire measurements of turbulence intensity, a desire arose to use crosswires, Dantec 55P61, to obtain *v'* and *w'* measurements. By measuring *v'* and *w'*, a sense of the vorticity present in the flow could be determined. Also, having performed many flights with the parallel array straight wires it was known that electronic noise is only a small

part of the flow and not a source of major concern. Since the dual wire probes installed for use with the parallel array straight wires could be used with crosswires, no modifications were needed to the sting mount or the data acquisition program. Correlations could also be performed to remove acoustic sound. However, changes were required to the MATLAB code that calculates turbulence intensities. Typically, in order to calibrate crosswires the probes are rotated to multiple known angles in order to determine the change in velocity relative to the angle changes. These calibrations allow for accurately determining the *v'* and *w'* components of the flow. While this is relatively easy procedure in a wind tunnel, it would be extremely difficult to implement in a flight environment. During the research dives performed in the aircraft, angle of sideslip could only be held to within ±0.1° and during the hotwire calibrations typically only to within ±0.5°. These ranges would not provide for very accurate calibrations, especially with the addition that the aircraft had a limited range of sideslip that could be safely flown. The other option would be to calibrate using aircraft angle of attack, but this is very hard to maintain and as such was not feasible. Because of the complications with performing the typical calibrations that would be used with a crosswire it was decided to use the same calibration scheme as was used for the straight wires, with the assumption that the wires were 45° to the freestream flow, and therefore calibrations were performed with velocities equal to the calculated freestream velocity divided by the square root of two. This method does not provide perfect results but rather results that can only be used to get an idea of the levels of *v'* and *w'*.

Another disadvantage the crosswires have was no way of removing electronic noise. With the parallel arrays, electronic noise could be remove because the wires were 0.4mm apart and parallel to each other. The crosswires did, however, have wires that were approximately the same distance apart, but the wires were angled 90° away from each other. Therefore, electronic noise could not be removed from the crosswire signals, but acoustic sound could be removed since two crosswire probes were used. This provided for removing acoustic sound the same as with the parallel wires. Also, it will be shown in the results section that this was an acceptable trade-off due to electronic noise being a relatively low part of the signal while acoustic sound was a very significant source.

While it will be shown that acoustic sound does enter into the signal, it is believed this was not the only content being removed through the correlations and being considered apart of acoustic sound. It has been noticed that the initial unseparated turbulence values were higher than previously measured either by Riedel and Stitzmann [16] or Carpenter [5]. Results higher than Carpenter's are especially of concern since those measurements were performed on the same platform, although changes were made including different wiring and filter. One theory is that crosstalk from the pressure transducers and temperature controller being sampled at high frequency on the same DAQ board as the hotwires. It has been confirmed that a very significant amount of noise was introduced into the pressure signals, as can be seen in Fig. 31. This measurement was taken in-flight at the same time and leads to the conclusion that significant amounts of noise were induced on the signals at 45kHz. However, it is also believed that the majority of this should be removed through the correlations. If the

signal was true electronic noise it would be removed as such in the correlations, but if it was something that was introduced on all of the signals simultaneously it would be removed as acoustic sound. Due to the high levels of acoustic sound the belief is that a similar disturbance was introduced on all of the signals simultaneously. Even though it is believed that this disturbance is removed through the correlations, it is desired not to have it in the signal at all.

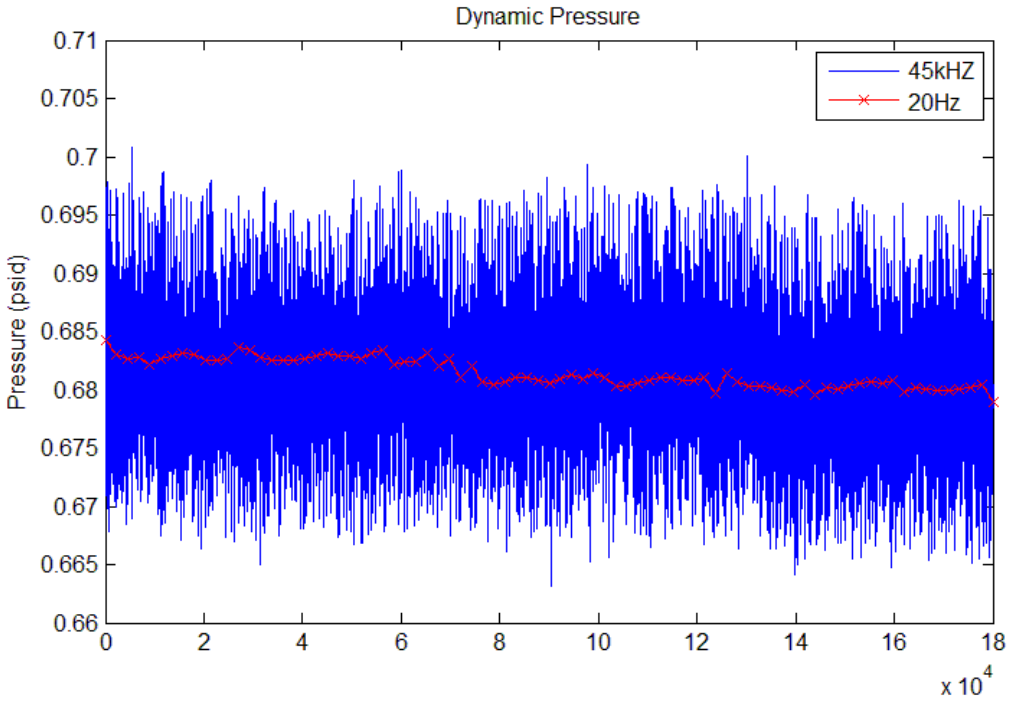

Fig. 31 Comparison of dynamic pressure sampled at 45kHz versus 20Hz simultaneously on separate DAQ boards.

Due to the way the data was acquired in-flight and the way the calibrations were performed, the hotwire measurements could be easily removed from the pressure and temperature measurements. In order to perform the calibrations, all of the pressure,

temperature, and hotwire measurements were averaged for each calibration point negating the need for measurements at 45kHz. Also, when making the actual measurements, the pressure and temperature were only used to correct the voltages for temperature and provide an initial guess for the velocity for the code to use. Therefore, an exact velocity corresponding to each hotwire voltage sampled at 45kHz is not needed, and the temperature already had a linear fit applied to it and that linear line was used to provide the temperature correction at each point.

All of the pressure and temperature data was already sampled at 20Hz; the only problem was aligning the data acquired at 20Hz with that acquired at 45kHz. It was decided the best way to do this would be just to write a separate file that contains only the pressure and temperature data and have the file's write function controlled by the writing of the 45kHz file. This prevents the need to compare timestamps in order to align the data. Implementing this solution should remove as much crosstalk as is possible from the hotwire signals. No in-flight measurements have been made with this change to the setup so there are no results to report as to its effect on the initial turbulence intensity measurements.

Results

This procedure to calculate atmospheric freestream turbulence intensities has been implemented on a number of flights already, and can be continuously run for future flights to get a better mean of the freestream turbulence along with any possible seasonal variances. Initial calculations were performed between about 10000-10500ft at a unit Reynold's number of 3.7x10^6 1/m. One of the biggest reasons for picking these

parameters was because they are completely within the calibration range of the hotwires. This allowed for measurements within the known calibration band and the calibration curves did not require extrapolation in order to perform the calculations. In the results so far, the average freestream turbulence intensity is 0.035% in a range from 0.023% - 0.047%. These results fall well under the values previously measured in the same geographic location on the same platform in the work done by Carpenter [5]. The current work has a similar, but slightly larger, range than reported by Carpenter, but the current work is approximately 0.02-0.03% lower. This result validates partly the need to in some way remove electronic noise and freestream sound from the measurements, at least on this platform. These results do however match very well with those found by Riedel and Sitzmann [16], with the exception that the current results have a range that is larger and goes to lower turbulence intensity values.

Statistical analysis was also performed on the data to determine how much the data deviated along with what amount of the original measured signal was actually velocity fluctuation and not electronic noise or acoustic sound. By performing a statistical analysis of the data points collected, the standard deviation over the population of the calculated freestream turbulence intensities was determined to be 0.009%. Analysis of the effectiveness and extent of the correlations on the data is also helpful. The average calculated freestream turbulence intensity prior to any correlations was 0.111% with a standard deviation of 0.053%. These particular statistics are an average and standard deviation based on all four wire used. In general, the measured turbulence intensities across all of the wires were close to each other for a particular flight, especially the two

wires in the same array. The average RMS intensity of the electronic noise in the signals that was removed by the correlations was 0.017%, while the average RMS intensity of the acoustic sound that was removed was 0.098%. Another comparison that was made was the ratio of the final freestream turbulence to both the electronic noise and acoustic sound whose average was 9.49 and 0.39, respectively. Both of the comparisons reveal that the biggest addition to the signals over the actual freestream turbulence was acoustic sound.

The freestream turbulence measurements were also shown to be repeatable during the course of the experiment. Two flights were performed one morning with the measurements coming approximately 3 hours and 15 minutes apart. While this amount of time was long enough for the atmosphere to change, it was short enough that the turbulence levels should be similar. In between the two flights the hotwires were removed, reinstalled, and retuned. Calibrations were also performed on both flights because the hotwires were removed. A comparison of the calculated turbulence intensity measurements between the earlier and the later flight revealed a change from 0.023% to 0.027%, respectively. This is only a minor change in turbulence intensity and can be easily attributed to changes in the atmosphere. An inversion layer was present at approximately 6000ft that day, and clouds had formed at that altitude in between the two flights. Also, the flight crew noticed the second flight was bumpier than the first. These results provide a good indication that the measurements performed during these experiments are repeatable, especially since the two flights both had a completely independent setup, tuning, and calibration.

Once the method was proven, hotwire measurements were taken during the entire extent of the research dive from 10000ft down to 3000ft. This allowed for taking hotwire measurements at the speeds and locations of where all of the flight research was being performed. One disadvantage to this was that the speeds were out of the calibration ranges. As was mentioned above, the highest velocity used during the calibration was *Re'* = 4.7x10^6 1/m. However, during the dive the speed was close to *Re'* = 5.5 x10^6 1/m which was significantly outside the calibration range and required extrapolating a fourth-order curve. These results were subject to some error, but taking the hotwire data during the research dive was of more value than for just turbulence measurements because it could be used to create a PSD plot in the event of unknown results during the experiment. These measurements have only been performed a minimal amount of time and thus there does not exist a large enough sample to get an average that is reportable. Measurements using crosswires have also begun, but they also are only to a minimal number of measurements and are not yet reportable.

It has been shown that acoustic sound contributes a very large portion of the original measured signal and finding its source and removing the source would provide significant value in measuring freestream turbulence intensity. One way to determine the source of the sound is to perform a PSD analysis and determine the frequency where any peaks are located. Figure 32 shows a PSD plot containing all four wires which shows how most of the peaks in the signal are shared by all four wires, even if their amplitude is slightly different. The largest peak occurs at 87Hz which is equivalent to a rotation of 5200RPM. During all of the hotwire measurements the aircraft's engines were operated

at 2600RPM and taking into consideration that the aircraft had a two-blade propeller the blade passing frequency was 5200RPM. The peaks located below about 3000Hz are all some harmonic or sub-harmonic of 87Hz. This reveals that the main source of sound in the signal came from the rotation of the propeller blades on the aircraft. A platform that can operate without running an engine while taking measurements (i.e. glider) would be of immense value in measuring freestream turbulence intensity.

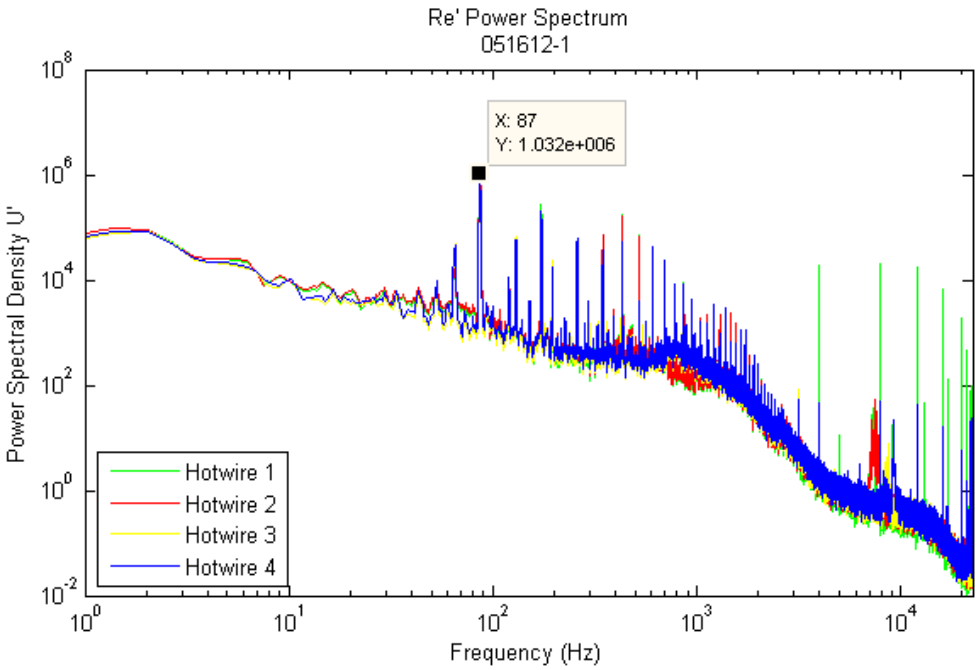

Fig. 32 Comparison of hotwire signals and determination of acoustic sound frequency.

CHAPTER VI

SUMMARY AND CONCLUSIONS

A plethora of work involving boundary layer stability and transition has been accomplished, even if there has only been a low level of success. While success in showing delay in transition has not been attained, much was learned to help the future researcher perform these types of experiments with greater ease. Plasma DREs have yet to be shown definitively effective or ineffective under conditions where other DREs worked. Thus, there is still the possibility that plasma DREs can be an effective method for LFC. Techniques have been developed to ease the installation, but there still exists much work to be done in order to get manufacturing and installation of plasma actuators to a level that is viable on any scale larger than in a research lab. While previous work done utilizing applique DREs has not been successfully repeated, lessons have been learned on ways to apply applique DREs with greater ease. However, even with these lessons, applique DREs are also not really a viable solution outside of a research lab, but can be an important tool in verifying an experimental setup if they are successful in delaying transition.

Great strides were made with success in regards to atmospheric turbulence measurements. An essentially turn-key setup has been put into place at the Texas A&M Flight Research Laboratory to use hotwires to measure freestream turbulence intensities. The original theory that turbulence in the flight environment is actually lower than previously measured has been confirmed. Through the use of temporal correlations to

remove both electronic noise and acoustic sound, a more accurate measurement of freestream turbulence has been achieved. A logical next step to these measurements is to take the techniques learned and implemented in this work and apply them to a platform that has low acoustic sound. This could be accomplished by a number of methods. The best solution would be the use of a glider, which contains no operating motor or propeller, as it would remove all external sources of acoustic noise. Another possible way to remove acoustic sound is through the use of a single engine aircraft. It is not known if this would be effective, but it is plausible that the acoustic sound levels measured by hotwires could be drastically reduced by removing both an engine and propeller from the experimental platform used in this research. However, the current setup for measurements was valuable in that it allowed for accurate measurements of freestream turbulence and will allow for knowing the turbulence level that corresponds to specific boundary layer stability experimental data points. This could potentially be invaluable information in determining why a technology works in one case but not in another. It's also invaluable information in being able to compare flight data to wind tunnel data.

REFERENCES

[1] Saric, W. S., "Boundary-Layer Stability and Transition," *Springer Handbook of Experimental Fluid Mechanics,* edited by C. Tropea, A. Yarin, J. Foss, Springer-Verlag, Berlin, Heidelberg, Part C, Chap. 12, Sec. 12.3, 2007, pp.886-96.

[2] Arnal, D., and Archambaud, J.P., "Laminar-turbulent transition control: NLF, LFC, HLFC," *Advances in Laminar-Turbulent Transition Modeling*, VKI Lecture Series. Brussels, Belgium: Von Karman Institute for Fluid Dynamics, 2009.

[3] Hunt, L. E., "Boundary-Layer Receptivity to Three-Dimensional Roughness Arrays on a Swept-Wing," Ph.D. Dissertation, Aerospace Engineering Dept., Texas A&M Univ., College Station, TX, 2011.

[4] Reed, H. L., and Saric, W. S., "Transition Mechanisms for Transport Aircraft," *AIAA Paper* 2008-3743, 2008.

[5] Carpenter, A. L., "In-Flight Receptivity Experiments on a 30-Degree Swept-Wing Using Micron-Sized Discrete Roughness Elements," Ph.D. Dissertation, Aerospace Engineering Dept., Texas A&M Univ., College Station, TX, 2009.

[6] Saric, W. S., Carillo Jr., R. B., and Reibert, M. S., "Leading-Edge Roughness as a Transition Control Mechanism," *AIAA Paper* 98-0781, 1998.

[7] Deyhle, H., and Bippes H., "Disturbance Growth in an Unstable Three-Dimensional Boundary Layer and Its Dependence on Initial Conditions," *Journal of Fluid Mechanics,* Vol. 316, 1996, pp. 73–113.

[8] Riebert M. S., Saric, W. S., Carillo Jr., R. B., and Chapman, K. L., "Experiments in Nonlinear Saturation of Stationary Crossflow Vortices in a Swept-Wing Boundary Layer," *AIAA Paper* 96-0184, 1996.

[9] Corke, T. C., Post, M. L., and Orlov, D. M., "Single Dielectric Barrier Discharge Plasma Enhanced Aerodynamics: Physics, Modeling, and Applications," *Experiments in Fluids*, Vol. 46, No. 1, 2008, pp. 1-26.

[10] Saric, W. S., and Reed, H. L., "Toward Practical Laminar Flow Control-Remaining Challenges," *AIAA Paper* 2004-2311, 2004.

[11] Schuele, C. Y., "Control of Stationary Cross-Flow Modes in a Mach 3.5 Boundary Layer Using Patterned Passive and Active Roughness," Ph.D. Dissertation, Aerospace and Mechanical Engineering Dept., University of Notre Dame, Notre Dame, IN, 2011.

[12] "Flight Test Measurement Techniques for Laminar Flow," Edited by D. Fisher, K.H. Horstmann and H. Riedel, RTO AG-300, Vol. 23 / SCI-040, 2003.

[13] Reshotko, E., Saric, W. S., and Nagib, H. M., "Flow Quality Issues for Large Wind Tunnels," *AIAA Paper* 97-0225, 1997.

[14] Saric, W. S., "Low-Speed Experiments: Requirements for Stability Measurements," *Instability and Transition,* edited by M. Y. Hussaini, R. G. Voight, Springer-Verlag, Vol. 1, 1990, pp. 162-176

[15] Saric, W. S., Takagi, S., and Mousseux, M., "The ASU Unsteady Wind Tunnel and Fundamental Requirements for Freestream Turbulence Measurements," *AIAA Paper* 88-0053, 1988.

[16] Riedel, H., and Sitzmann, M., "In-Flight Investigations of Atmospheric Turbulence," *Aerospace Science and Technology*, No. 5, 1997, pp. 301-19.

[17] Saric, W. S., and Reshotko, E., "Review of Flow Quality Issues in Wind Tunnel Testing," *AIAA Paper* 98-2613, 1998.

[18] Woodruff, M. J., "Receptivity Studies on an Swept-Wing Model," Master Thesis, Aerospace Engineering Dept., Texas A&M Univ., College Station, TX, 2011.

[19] Craig, S. A., Humble, R. A., and Saric, W. S., "Characterization of the Flowfield Structure of an Annular Dielectric Barrier Discharge Plasma Actuator," *AIAA Paper* 2011-3987, 2011.

[20] White, E. B., "Breakdown of Crossflow Vortices," Ph.D. Dissertation. Arizona State University, Tempe, AZ, 2000.

[21] Bearman, P. W., "Corrections for the Effect of Ambient Temperature Drift on Hot-Wire Measurements in Incompressible Flow," *DISA Information*, No. 11, 1971, pp. 25-30.

[22] "Supplemental Oxygen", *Code of Federal Regulations*, Title 14, Part 91.211, 1963.

[23] Naguib, A. M., Gravante, S. P., and Wark, C. E., "Extraction of Turbulent Wall-Pressure Time-Series Using an Optimal Filtering Scheme," *Experiments in Fluids*, Vol. 22, No. 1, 1996, pp. 14-22.